

# Homogenization of Maxwell's equations in periodic composites

**Vadim A. Markel** <sup>‡</sup>

Department of Radiology and Graduate Group in Applied Mathematics and  
Computational Science, University of Pennsylvania, Philadelphia, PA 19104

**John C. Schotland** <sup>§</sup>

Department of Mathematics, University of Michigan, Ann Arbor, MI 48109

**Abstract.** We consider the problem of homogenizing the Maxwell equations for periodic composites. The analysis is based on Bloch-Floquet theory. We calculate explicitly the reflection coefficient for a half-space, and derive and implement a computationally-efficient continued-fraction expansion for the effective permittivity. Our results are illustrated by numerical computations for the case of two-dimensional systems. The homogenization theory of this paper is designed to predict various physically-measurable quantities rather than to simply approximate certain coefficients in a PDE.

<sup>‡</sup> E-mail: vmarkel@mail.med.upenn.edu

<sup>§</sup> E-mail: schotland@umich.edu

## 1. Introduction

Theories of electromagnetic homogenization of composite materials—also known as effective medium theories (EMTs)—have a history which goes back to the time of J.C. Maxwell. Nevertheless, these theories continue to attract attention and even controversy, as is evidenced by the recent review by Simovski [1] and many references therein. Interest in EMTs has been steadily on the rise for the past ten years. One can conclude that the questions of how to choose a physically-relevant and computationally-efficient EMT and what are its limits of applicability have not been completely settled. This paper is an attempt to answer the questions posed above for periodic composites; random media will not be considered.

It is useful to recognize from the outset that all EMTs can be classified as either *standard* or *extended*. A standard EMT is obtained by taking the limit  $h \rightarrow 0$ , where  $h$  is the scale of the medium's heterogeneity; in this paper,  $h$  is the lattice period. In standard theories,  $h$  is viewed as a mathematically- and physically-independent variable and the resulting effective medium parameters are independent of  $h$ , as long as the latter is small enough for the theory to be applicable. Another feature of all standard theories is the so-called law of unaltered ratios [2], which states that, if a composite medium is made of several constituents with permittivities  $\epsilon_j$  ( $j = 1, 2, \dots$ ), and if  $\epsilon_j \rightarrow \lambda \epsilon_j$  ( $\lambda > 0$ ), then the effective permittivity  $\epsilon^{\text{eff}}$  also scales as  $\epsilon^{\text{eff}} \rightarrow \lambda \epsilon^{\text{eff}}$ .

Extended EMTs came to the fore in the works of Niklasson *et al.* [3] and Doyle [4]. The basic idea of these papers is to note that one can compute the exact electric and magnetic polarizabilities,  $\alpha_e$  and  $\alpha_m$ , of a spherical particle through the use of the first Lorenz-Mie coefficients,  $a_1$  and  $b_1$ , even when the sphere in question is not small compared to the external wavelength ¶. These polarizabilities can be used to construct an “extended” Maxwell-Garnett approximation. Since  $a_1$  and  $b_1$  are not proportional to the sphere volume, except in the quasistatic limit, the resultant EMTs contain the sphere radius explicitly and, therefore, violate the two essential properties of standard EMTs described above.

In a more general setting, an extended EMT can be obtained by considering the material parameters of the composite constituents as being dependent on  $h$ , and then taking the limit  $h \rightarrow 0$ . This approach is exemplified by the work of Felbacq and Bouchitte [5], where it is assumed that the permittivity of one of the constituents scales as  $1/h^2$ . This theory does not really assume a *physical* dependence of the material parameters on  $h$  but rather aims at describing a given composite by means of considering a hypothetical composite in which the material parameters of the constituents depend on  $h$  in a prescribed manner and requiring that, for some particular value of  $h$ , the hypothetical and the real composites coincide. However, there exist an infinite number of such hypothetical systems with different dependencies of the material parameters on

¶ The magnetic dipole moment of any particle depends on the choice of reference frame if the particle has a nonzero electric dipole moment. The Lorenz-Mie coefficient  $b_1$  gives the magnetic dipole moment of a sphere in a reference frame whose origin coincides with the sphere center.

*h.* Taking the limit  $h \rightarrow 0$  in each of these systems would naturally lead to a different homogenization result and error. The question then is whether the effective medium parameters obtained by using extended EMTs have the same physical meaning as the conventional parameters of homogeneous media.

Critical analyses of extended EMTs have been performed by several authors [6–9]. The common conclusion of these papers appears to be that the range of validity of the extended theories is limited. For example, one limitation is revealed by examining the angular dependence of the reflection and transmission coefficients at a flat interface. Typically, one is interested in comparing the coefficients measured or computed without any approximations to those derived from an EMT. While reasonable agreement can be obtained close to the normal direction of incidence, extended EMTs usually fail to reproduce the full angular dependence, especially, when incident evanescent waves are included [9]. Bohren has commented [6] that the agreement at normal incidence comes as no surprise: an extended theory has two adjustable complex-valued parameters (the effective permittivity and permeability), which is sufficient to fit the two measurable quantities (the transmission and reflection coefficients for the normal incidence) regardless of the validity of the underlying approximation.

One way of dealing with the above-mentioned issues, without abandoning the extended EMTs altogether, is to allow the effective medium parameters to be spatially dispersive [10,11]. Spatial dispersion is, indeed, a great rescuer, as it allows one to fit any angular dependence of the transmission and reflection coefficients to the predictions of an EMT by means of introducing incidence-angle-dependent effective medium parameters. Whether this can be interpreted as true nonlocality or merely as an effect of the medium not being electromagnetically homogeneous is not clear [12]. One problem with nonlocality is that it complicates the solution of boundary value problems and another is that it destroys important or interesting physical effects, including the optical superresolution of the type proposed by Pendry [13]. Since a strong argument against the use of spatially-nonlocal EMTs can be made, we will not explore this possibility further.

Another feature by which EMTs can be classified is the physical model of the medium. In the model of dipole lattices, the medium is thought of as being composed of point particles which are completely characterized by their polarizabilities (electric and, possibly, magnetic) and whose shape and size do not enter into the problem directly [14–16]. Alternatively, one can consider the space as a two-component continuous medium [17–19]. The point-dipole model is appealing because of its simplicity but leads to serious mathematical problems. The so-called dipole sum (also known as the lattice sum or the dipole self-energy), which plays a key role in this model, diverges in the case of three-dimensional lattices. While it is true that even divergent series can be summed by means of applying various mathematical tricks, the results obtained depend on the particular trick used, a state of affairs that is not very satisfying. Therefore, we will adopt from the start a model of a two-component continuous medium. As the development in this paper progresses, it will become apparent why the point-

dipole model is inadequate.

The theoretical framework in this paper is similar to that employed by Krokhin *et al.* [20,21] for the homogenization of two-dimensional periodic composites. In both cases, the analysis is based on Floquet-Bloch theory. However, in several aspects, we go beyond the results obtained by Krokhin *et al.* In particular, we consider both two-dimensional and three-dimensional composites, compute explicitly the reflection coefficient for a half-space, and derive and implement a computationally-efficient continued-fraction expansion for the effective permittivity. There are also some methodological differences. Specifically, we make use of the integral equation formulation of scattering theory for the Maxwell equations rather than solving boundary value problems, which results in a different mathematical structure of some of the obtained formulas. Also, an important feature of this work, which distinguishes it from certain mathematical approaches to homogenization, is that we seek to approximate physically-measurable quantities (such as the reflection coefficient) rather than coefficients in a PDE.

The mathematical development in this paper begins by considering the integral equation obeyed by the polarization field, which is introduced in Sec. 2. In Sec. 3, we derive a homogenization theory of the standard type for infinite periodic media. Reflection and refraction at a planar boundary is considered in Sec. 4. In Sec. 5, we discuss the correspondence between the point-dipole model and the continuous-medium model of this paper. One mathematically-novel element of the theory developed herein is a continued-fraction expansion of the effective permittivity, which is derived in Sec. 6 and used in the numerical simulations of Sec. 7. The expansion has its origins in a theorem on resolvents of general linear operators (with no special symmetry properties), which is stated in Sec. 6 and proved in the appendices. A discussion and a brief summary of results are contained in Secs. 8 and 9.

## 2. Basic equations

The geometry of the problem we consider is sketched in Fig. 1. The medium consists of two intrinsically non-magnetic constituents: a host medium of permittivity  $\epsilon_b$  and periodically-arranged inclusions of permittivity  $\epsilon_a$ . In practice, the host is often a transparent dielectric with  $\text{Re}\epsilon_b > 0$ ,  $0 < \text{Im}\epsilon_b \ll \text{Re}\epsilon_b$ , and the inclusions are metallic. However, the theory of this paper places no such restriction on the permittivities and only requires that  $\text{Im}\epsilon_b > 0$ ,  $\text{Im}\epsilon_a > 0$ . In the case when the host medium is vacuum, we will take  $\epsilon_b = 1 + i0$ . The inclusions are arranged on a cubic lattice of period  $h$ . The position vector of the center of each unit cell is denoted by  $\mathbf{r}_n$ , where  $n$  can be viewed as a composite index:  $n = (n_x, n_y, n_z)$  and  $\mathbf{r}_n = h(\hat{\mathbf{x}}n_x + \hat{\mathbf{y}}n_y + \hat{\mathbf{z}}n_z)$ . Whenever a summation over  $n$  (or a similar composite index  $m$ ) appears in the text, it is implied that the sum runs over all three integer indexes. Inside the  $n$ th cell, the spatial region  $\Omega_n$  has the permittivity  $\epsilon_a$ , and the rest of the cell has the background permittivity  $\epsilon_b$ . All regions  $\Omega_n$  are identical and only differ by translation. It is assumed that  $\Omega_n$  can touch but not cross the cell boundaries. No assumption on the connectivity of  $\Omega_n$  is

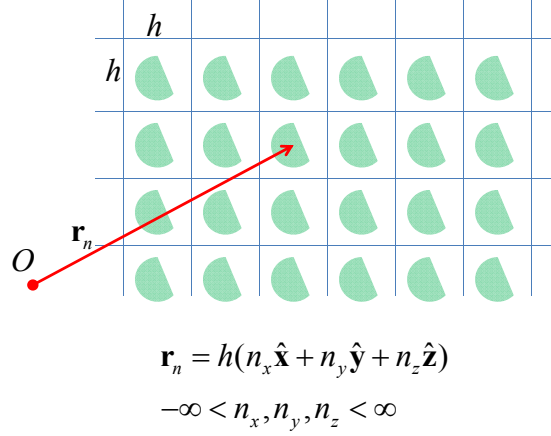


**Figure 1.** (color online) Sketch of the geometry considered: an infinite 3D lattice.

made. The union of all regions  $\Omega_n$  is denoted by  $\Omega_{\text{tot}}$  and the volume of each region by  $V$ :

$$\Omega_{\text{tot}} = \bigcup_n \Omega_n, \quad \int_{\Omega_n} d^3r = V. \quad (1)$$

We work in the frequency domain and the common factor  $\exp(-i\omega t)$  is suppressed. All frequency-dependent quantities, such as the permittivities  $\epsilon_b$  and  $\epsilon_a$ , are evaluated at the frequency  $\omega$ . The mathematical development in this paper begins with the integral equation

$$\mathbf{P}(\mathbf{r}) = \frac{3\chi}{4\pi} \left[ \mathbf{E}_i(\mathbf{r}) + \int_{\Omega_{\text{tot}}} G(\mathbf{r}, \mathbf{r}') \mathbf{P}(\mathbf{r}') d^3r' \right], \quad \mathbf{r} \in \Omega_{\text{tot}}. \quad (2)$$

Here  $\mathbf{P}(\mathbf{r})$  is the vector of “polarization”, which is related to the electric field  $\mathbf{E}(\mathbf{r})$  by

$$\mathbf{P}(\mathbf{r}) = \frac{\epsilon(\mathbf{r}) - \epsilon_b}{4\pi\epsilon_b} \mathbf{E}(\mathbf{r}), \quad (3)$$

$\mathbf{E}_i(\mathbf{r})$  is the incident electric field,  $G(\mathbf{r}, \mathbf{r}')$  is the *regular* part of the free-space, retarded Green’s tensor, and

$$\chi = \frac{\epsilon_a - \epsilon_b}{\epsilon_a + 2\epsilon_b}. \quad (4)$$

Note that  $\mathbf{P}(\mathbf{r})$  defined in (3) is not the true physical polarization, which is given by  $[(\epsilon(\mathbf{r}) - 1)/4\pi] \mathbf{E}(\mathbf{r})$ , but rather an auxiliary field; it vanishes in the host medium.

In what follows, we will make use of the spatial Fourier transform of the Green’s tensor, namely,

$$G(\mathbf{r}, \mathbf{r}') = \frac{4\pi}{3} \int \frac{d^3p}{(2\pi)^3} K(\mathbf{p}) \exp[i\mathbf{p} \cdot (\mathbf{r} - \mathbf{r}')] , \quad (5)$$

where

$$K(\mathbf{p}) = \frac{2k_0^2 + p^2 - 3\mathbf{p} \otimes \mathbf{p}}{p^2 - k_0^2} , \quad (6)$$

and

$$k_0 = \sqrt{\epsilon_b} \omega / c \quad (7)$$

is the wave number in the host medium. We note that the integral equation (2) is equivalent to the pair of curl Maxwell equations written in the frequency domain.

### 3. Waves in infinite lattices

#### 3.1. Three-dimensional lattices

Consider the propagation of a wave in a three-dimensional infinite lattice. In this case, the incident field is absent and Eq. (2) must be satisfied for  $\mathbf{E}_i = 0$ . We seek the solution to Eq. (2) in the form of a Bloch wave:

$$\mathbf{P}(\mathbf{r}) = \exp(i\mathbf{q} \cdot \mathbf{r}_n) \mathbf{F}(\mathbf{r} - \mathbf{r}_n) , \quad \mathbf{r} \in \Omega_n . \quad (8)$$

Here  $\mathbf{q}$  is the Bloch wave number and  $\mathbf{F}(\mathbf{r})$  is a vector function. Equivalently, if we write  $\mathbf{r} = \mathbf{r}_n + \mathbf{R}$ , then

$$\mathbf{P}(\mathbf{r}_n + \mathbf{R}) = \exp(i\mathbf{q} \cdot \mathbf{r}_n) \mathbf{F}(\mathbf{R}) , \quad \mathbf{R} \in \Omega . \quad (9)$$

In this formula,  $\Omega \equiv \Omega_0$  is the region centered at the origin of a rectangular reference frame. From the above relation, we find the equation obeyed by  $\mathbf{F}(\mathbf{R})$ :

$$\mathbf{F}(\mathbf{R}) = \frac{3\chi}{4\pi} \int_{\Omega} W(\mathbf{R}, \mathbf{R}') \mathbf{F}(\mathbf{R}') d^3 R' , \quad (10)$$

where

$$W(\mathbf{R}, \mathbf{R}') = \sum_m G(\mathbf{r}_n + \mathbf{R}, \mathbf{r}_m + \mathbf{R}') \exp[i\mathbf{q} \cdot (\mathbf{r}_m - \mathbf{r}_n)] . \quad (11)$$

It can be seen that  $W$  is independent of  $n$ . It should also be noted that the summation in Eq. (11) runs over the entire lattice, including the term  $m = n$ . In theories that consider point-like particles, the dipole sum is defined as an incomplete lattice sum, which excludes the term  $m = n$ . This precludes direct application of the Poisson summation formula and unnecessarily complicates the mathematics [16].

Returning to our derivation, we evaluate  $W$  as

$$\begin{aligned}
W(\mathbf{R}, \mathbf{R}') &= \frac{4\pi}{3} \int \frac{d^3p}{(2\pi)^3} K(\mathbf{p}) \exp[i\mathbf{p} \cdot (\mathbf{R} - \mathbf{R}')] \sum_m \exp[i(\mathbf{p} - \mathbf{q}) \cdot (\mathbf{r}_n - \mathbf{r}_m)] \\
&= \frac{4\pi}{3h^3} \sum_{\mathbf{g}} K(\mathbf{q} + \mathbf{g}) \exp[i(\mathbf{q} + \mathbf{g}) \cdot (\mathbf{R} - \mathbf{R}')] , 
\end{aligned} \tag{12}$$

where

$$\mathbf{g} = (2\pi/h)(\hat{\mathbf{x}}n_x + \hat{\mathbf{y}}n_y + \hat{\mathbf{z}}n_z) \tag{13}$$

are the reciprocal lattice vectors and we have used the Poisson summation formula

$$\sum_m \exp[i(\mathbf{p} - \mathbf{q}) \cdot (\mathbf{r}_m - \mathbf{r}_n)] = \left(\frac{2\pi}{h}\right)^3 \sum_{\mathbf{g}} \delta(\mathbf{p} - \mathbf{q} - \mathbf{g}) . \tag{14}$$

The summation in Eqs. (12),(14) is over the complete set of reciprocal lattice vectors; equivalently, it can be viewed as summation over the triplet of indexes  $(n_x, n_y, n_z)$  which appear in (13).

The series in the right-hand side of (12) diverges when  $\mathbf{R} = \mathbf{R}'$ . This is the well-known divergence of the dipole sum [22] which hinders the analysis of waves in lattices made of point-like polarizable particles. The model of point-like dipoles is discussed in more detail in Sec. 5. In the equations derived above, the divergence is of no concern because  $W(\mathbf{R}, \mathbf{R}')$  appears only inside an integral and the singularity in question is integrable.

Upon substitution of (12) into (10), we obtain

$$\mathbf{F}(\mathbf{R}) = \frac{\chi}{h^3} \sum_{\mathbf{g}} K(\mathbf{q} + \mathbf{g}) \exp[i(\mathbf{q} + \mathbf{g}) \cdot \mathbf{R}] \int_{\Omega} \mathbf{F}(\mathbf{R}') \exp[-i(\mathbf{q} + \mathbf{g}) \cdot \mathbf{R}'] d^3R' . \tag{15}$$

It follows from (15) that  $\mathbf{F}(\mathbf{R})$  can be expanded as

$$\mathbf{F}(\mathbf{R}) = \sum_{\mathbf{g}} \mathbf{F}_{\mathbf{g}} \exp[i(\mathbf{q} + \mathbf{g}) \cdot \mathbf{R}] \tag{16}$$

and that the expansion coefficients satisfy the system of equations

$$\mathbf{F}_{\mathbf{g}} = \rho\chi K(\mathbf{q} + \mathbf{g}) \sum_{\mathbf{g}'} M(\mathbf{g} - \mathbf{g}') \mathbf{F}_{\mathbf{g}'} , \tag{17}$$

where  $\rho = V/h^3$  is the volume fraction of inclusions and  $M(\mathbf{g})$  is defined by the expression

$$M(\mathbf{g}) = \frac{1}{V} \int_{\Omega} \exp(-i\mathbf{g} \cdot \mathbf{R}) d^3R . \tag{18}$$

Note that  $M(\mathbf{g})$  is defined only by the shape of the inclusions and is invariant with respect to the coordinate rescaling  $\mathbf{r} \rightarrow \lambda \mathbf{r}$ . Some mathematical properties and calculations of  $M(\mathbf{g})$  for special geometries are given in Appendix A.

So far, we have simply restated the well known theorem of Floquet. The eigenproblem (17) defines the band structure of a photonic crystal. It is well known that EMTs are not always applicable to photonic crystals. However, there exists a regime in which effective medium parameters can be reasonably introduced, and this regime will be explored below. Namely, if  $qh, k_0h \ll 1$ , we can consider the cases  $\mathbf{g} = 0$  and  $\mathbf{g} \neq 0$  in (17) separately. This yields the following equations:

$$\mathbf{F}_0 = \rho\chi K(\mathbf{q}) \left[ \mathbf{F}_0 + \sum_{\mathbf{g} \neq 0} M(-\mathbf{g}) \mathbf{F}_{\mathbf{g}} \right], \quad (19a)$$

$$\mathbf{F}_{\mathbf{g}} = \rho\chi Q(\mathbf{g}) \left[ M(\mathbf{g}) \mathbf{F}_0 + \sum_{\mathbf{g}' \neq 0} M(\mathbf{g} - \mathbf{g}') \mathbf{F}_{\mathbf{g}'} \right], \quad \mathbf{g} \neq 0, \quad (19b)$$

where

$$Q(\mathbf{g}) \equiv \lim_{h \rightarrow 0} K(\mathbf{q} + \mathbf{g}) = 1 - 3\hat{\mathbf{g}} \otimes \hat{\mathbf{g}}, \quad \mathbf{g} \neq 0.$$

Here  $\hat{\mathbf{g}} = \mathbf{g}/|\mathbf{g}|$  is a unit vector.

The derivation of Eqs. (19) is one of the key developments of this paper. It can be seen that the equations in (19b) do not contain the variables  $k_0$  or  $\mathbf{q}$ , but are completely defined by the geometry of inclusions and by the variable  $\chi$ . Moreover, these equations are invariant with respect to the rescaling  $\mathbf{r} \rightarrow \lambda \mathbf{r}$ . For any given value of  $\mathbf{F}_0$ , (19b) can be solved uniquely as  $\mathbf{F}_{\mathbf{g}} = T_{\mathbf{g}} \mathbf{F}_0$ , where the tensors  $T_{\mathbf{g}}$  are determined by the shape of inclusions and by  $\chi$ . Given this result, we can write

$$\sum_{\mathbf{g} \neq 0} M(-\mathbf{g}) \mathbf{F}_{\mathbf{g}} = \sum_{\mathbf{g} \neq 0} M(-\mathbf{g}) T_{\mathbf{g}} \mathbf{F}_0 = \Sigma \mathbf{F}_0, \quad (20)$$

where the tensor  $\Sigma$  has all the properties of the tensors  $T_{\mathbf{g}}$  and, in addition, is independent of  $\mathbf{g}$ . It will be shown in Sec. 6 that  $\Sigma$  plays the role of the self-energy and originates due to the electromagnetic interaction within and between the inclusions.

Using the notation introduced in (20), we can rewrite (19a) as

$$[1 - \rho\chi K(\mathbf{q})(1 + \Sigma)] \mathbf{F}_0 = 0. \quad (21)$$

This equation has nontrivial solutions if

$$\det [1 - \rho\chi K(\mathbf{q})(1 + \Sigma)] = 0. \quad (22)$$

The quantity in the square brackets is a  $3 \times 3$  matrix. Its eigenvectors determine the polarization eigenstates. The effective medium parameters can be obtained by



considering the dependence of  $\mathbf{q}$  on  $k_0$  for each eigenstate. Evidently, it is not possible to determine the effective permittivity  $\epsilon^{\text{eff}}$  and the effective permeability  $\mu^{\text{eff}}$  from consideration of the dispersion equation alone. For example, in an isotropic medium, only the product of these two quantities (the squared refractive index) can be unambiguously obtained. To determine  $\epsilon^{\text{eff}}$  and  $\mu^{\text{eff}}$  separately, one must consider reflection and refraction at the medium boundary. This will be done in Sec. 4. In particular, it will be shown that, in order to obtain the correct Fresnel reflection coefficients, one must set  $\mu^{\text{eff}} = 1$ .

In summary, the electromagnetic modes of the medium can be found if the tensor  $\Sigma$  is known. Computation of the modes involves diagonalization of a  $3 \times 3$  matrix, while the tensor  $\Sigma$  is uniquely determined by the solution to Eqs. (19b). The latter is an infinite set of equations which must be appropriately truncated in numerical computations. Thus, we have reduced the homogenization problem to solving a set of algebraic equations in which the shape of the inclusions appears only in the functions  $M(\mathbf{g})$ .

### 3.2. Special case: A medium whose optical and crystallographic axes coincide

The principal axes of the tensor  $\Sigma$  do not always coincide with the crystallographic axes of the medium. However, whenever such a coincidence occurs, the problem is simplified. The tensor  $\Sigma$  is diagonal in the reference frame defined by the crystallographic axes (which is the laboratory frame in this paper) if and only if the inclusions are symmetric with respect to reflections in each of the  $xy$ ,  $xz$  and  $yz$  planes. The principal values of  $\Sigma$  are not necessarily equal in this case. The two familiar examples of reflection-symmetric inclusions which result in all three principal values being different are a general parallelepiped and an ellipsoid with unequal semi-axes. However, if the inclusions also have cubic symmetry (which, in addition to reflections, includes rotations about each axis by the angle  $\pi/4$ ), then  $\Sigma$  is reduced to a scalar and the effective medium is isotropic.

If  $\Sigma$  is diagonal in the laboratory frame, a plane wave can propagate along each crystallographic axis and there exist three polarization states for each propagation direction. Consider a mode propagating along the axis  $\beta$  and linearly polarized along the axis  $\alpha$ . The indices  $\alpha$  and  $\beta$  label the Cartesian components of vectors and can take the values  $x$ ,  $y$  or  $z$ . If  $\alpha$  and  $\beta$  are two orthogonal directions, we have  $\mathbf{q} \cdot (1 + \Sigma)\mathbf{F}_0 = (1 + \Sigma_{\alpha\alpha})\mathbf{q} \cdot \mathbf{F}_0 = 0$ . Here  $\Sigma_{\alpha\alpha}$  denotes a principal value of  $\Sigma$ . Under the condition  $\mu^{\text{eff}} = 1$  (see discussion in the end of Sec. 3.1 and a rigorous proof in Sec. 4), we can write  $k_0^2 \epsilon_{\alpha\alpha}^{\text{eff}} = q^2 \epsilon_b$ . Upon substitution of this expression into (22) and taking into account the equality  $\mathbf{q} \cdot (1 + \Sigma)\mathbf{F}_0 = 0$ , we arrive at

$$\epsilon_{\alpha\alpha}^{\text{eff}} = \epsilon_b \frac{1 + 2\rho\chi(1 + \Sigma_{\alpha\alpha})}{1 - \rho\chi(1 + \Sigma_{\alpha\alpha})}. \quad (23)$$

Eq. (23) gives the effective permittivity for transverse modes of the effective medium. It can be seen that the Maxwell-Garnett mixing formula is obtained from (23) by setting  $\Sigma = 0$ . Electromagnetic interactions result in a nonzero value of  $\Sigma$  and, correspondingly,

in the deviation of the effective medium parameters from the predications of Maxwell-Garnett theory.

In addition to the two transverse modes, a longitudinally-polarized mode can also exist under certain conditions. A mode with an arbitrary wave number  $q$ , which propagates and is polarized along the same axis  $\alpha$ , exists if and only if

$$1 + 2\rho\chi(1 + \Sigma_{\alpha\alpha}) = 0. \quad (24)$$

From the property (A.4), it follows that  $\lim_{\rho \rightarrow 1} \Sigma_{\alpha\alpha} = 0$ . Consequently, the longitudinal waves exist in the high-density limit if  $1 + 2\chi = 0$ , which is only possible if  $\epsilon_a = 0$ . This is the well-known condition for longitudinal waves in a plasma. The low-density limit can not be considered so easily because  $\Sigma_{\alpha\alpha}$  does not approach zero when  $\rho \rightarrow 0$  (see the Sec. 3.3) and can, in fact, diverge for certain values of  $\chi$ . However, we can use the reciprocity substitution  $\rho \leftrightarrow 1 - \rho$ ,  $\epsilon_a \leftrightarrow \epsilon_b$  to see that, in the low-density limit, the condition for existence of longitudinal waves is  $\epsilon_b = 0$ .

We now discuss a more general case when  $\mathbf{q}$  lies in the  $xz$  plane. Problems of this type arise when one considers reflection and refraction at the interface  $z = 0$ , where the  $xz$ -plane is the plane of incidence, as is shown in Fig. 2. As will be discussed in much more detail in Sec. 4, the tangential component of the Bloch wave vector is, in this case, the same as that of the incident wave. Consequently, one can write  $\mathbf{q} = k_x \hat{\mathbf{x}} + q_z \hat{\mathbf{z}}$ . Here  $k_x$  is the projection of the incident wave vector onto the interface. The problem then consists in finding the eigenvalues of  $q_z$  and the corresponding polarization states  $\mathbf{F}_0$  for a fixed  $k_x$ . The case of s-polarization, when both  $\mathbf{F}_0$  and  $\Sigma \mathbf{F}_0$  are perpendicular to the plane of incidence, is trivial and will not be considered here. However, the case of p-polarization is somewhat more involved and requires further consideration.

Let  $\mathbf{F}_0 = F_{0x} \hat{\mathbf{x}} + F_{0z} \hat{\mathbf{z}}$ . Under the assumption of this subsection, namely, that the crystallographic and the optical axes coincide, we also have  $\Sigma \mathbf{F}_0 = \Sigma_{xx} F_{0x} \hat{\mathbf{x}} + \Sigma_{zz} F_{0z} \hat{\mathbf{z}}$ . Upon substitution of this expression into (22), one arrives at a  $2 \times 2$  eigenproblem. The corresponding matrix can have either one or two linearly-independent eigenvectors, which determine the polarization states. We can seek one of the eigenvectors in the form  $\mathbf{F}_0 = \lambda \mathbf{q}$ , where  $\lambda$  is a scalar. Obviously, if such an eigenvector exists, it corresponds to the longitudinally-polarized mode. However,  $\lambda \mathbf{q}$  is an eigenvector only if  $\det[1 + 2\rho\chi(1 + \Sigma)] = 0$ . In most practical cases, this condition can not be satisfied. Then the matrix in question is defective (it has only one linearly-independent eigenvector). This eigenvector can be determined by multiplying Eq. (22) by  $q^2 - k_0^2$ , writing  $q^2 = k_x^2 + q_z^2$  and solving the resultant quadratic equation with respect to  $q_z^2$ . This yields the following two roots:

$$q_z^2 = \epsilon_{xx}^{\text{eff}} k_0^2 - \frac{\epsilon_{xx}^{\text{eff}}}{\epsilon_{zz}^{\text{eff}}} k_x^2, \quad (25a)$$

$$q_z^2 = k_0^2 - k_x^2, \quad (25b)$$

where  $\epsilon_{\alpha\alpha}^{\text{eff}}$  is given by (23). The second root must be discarded because it has appeared only due to the multiplication of (22) by the factor  $q^2 - k_0^2$ ; the latter operation was used to bring the equation to polynomial form. However, the first solution is the well-known dispersion relation for an anisotropic medium whose permittivity tensor is diagonal in the laboratory frame and has the principal values of  $\epsilon_{\alpha\alpha}^{\text{eff}}$ .

We now find the polarization state which corresponds to the eigenvalue (25a). A straightforward calculation results in the following ratio:

$$\frac{F_{0x}}{F_{0z}} = -\frac{1 + 2\rho\chi(1 + \Sigma_{zz})}{1 + 2\rho\chi(1 + \Sigma_{xx})} \frac{q_z}{k_x}. \quad (26)$$

In the above equation,  $q_z$  is determined by taking the square root of the right-hand side of (25a), the branch being determined by the condition that the Bloch wave decays exponentially in the direction of propagation. Eq. (26) will be used below in Sec. 4 to compute the half-space reflection coefficient.

### 3.3. Low-density and low-contrast limits

Iteration of Eq.(19b) results in the following expansion for the self-energy:

$$\Sigma = \rho\chi \sum_{\mathbf{g} \neq 0} M(-\mathbf{g})Q(\mathbf{g})M(\mathbf{g}) + (\rho\chi)^2 \sum_{\mathbf{g}, \mathbf{g}' \neq 0} M(-\mathbf{g})Q(\mathbf{g})M(\mathbf{g}-\mathbf{g}')Q(\mathbf{g}')M(\mathbf{g}') + \dots \quad (27)$$

It is important to note that this expansion should be used with caution. Indeed, if  $\chi$  is of the order of unity or larger, the series in (27) does not converge, even for arbitrarily small values of the density  $\rho$ . This result may seem unexpected, but it is easily understood by observing that the functions  $M(\mathbf{g})$  depend on  $\rho$  and obey the sum rules (A.2).

In Sec. 6, a more useful (and always convergent) expansion of  $\Sigma$  will be derived. Here we note that the functions  $M(\mathbf{g})$  are independent of  $\chi$ . Therefore, (27) is the formal expansion of  $\Sigma$  into the powers of  $\chi$ . Thus, in the low-contrast limit ( $\chi \rightarrow 0$ ), we have  $\Sigma \rightarrow \rho\chi\sigma_1$ , where  $\sigma_1 = \sum_{\mathbf{g} \neq 0} M(-\mathbf{g})Q(\mathbf{g})M(\mathbf{g})$ . In the case of three-dimensional inclusions with cubic symmetry,  $\sigma_1$  is identically zero. Then the first non-vanishing term in the low-contrast expansion of  $\Sigma$  is given by  $(\rho\chi)^2\sigma_2$ , where  $\sigma_2$  grows naturally out of the second term in the right-hand side of (27).

### 3.4. Two-dimensional lattices

Consider a medium in which  $\epsilon = \epsilon(x, y)$  is independent of the  $z$  coordinate. As above, we assume that  $\epsilon(x, y)$  is periodic on a square lattice with lattice step  $h$ . The homogenization theory for this medium can be obtained either by considering a three-dimensional lattice with unequal steps  $h_x, h_y, h_z$  and taking the limit  $h_z \rightarrow 0$ , or by following the derivations of Sec. 3.1, taking account of the modified geometry. The results obtained are very similar to those in the 3D case, with some obvious modifications. Specifically, we arrive at Eqs. (19a),(19b) in which, however, we must

take  $\mathbf{g} = (2\pi/h)(\hat{\mathbf{x}}n_x + \hat{\mathbf{y}}n_y)$ . Additionally, in the integrals (18),  $\Omega$  must be understood as a two-dimensional region (the intersection of an inclusion with the  $xy$ -plane),  $V$  as the area of  $\Omega$ , and  $d^3R$  is replaced by  $d^2R$ . The definition of  $Q(\mathbf{g})$  (20) remains unchanged, but  $Q(\mathbf{g})$  is now a  $2 \times 2$  tensor.

Consider a wave propagating in the  $xy$  plane and polarized along the  $z$ -axis. In this case,  $\mathbf{F}_{\mathbf{g}} = \hat{\mathbf{z}}F_{\mathbf{g}}$ , where  $F_{\mathbf{g}}$  is a scalar and  $\Sigma$  can be found analytically in general. Indeed, we have in this case  $Q(\mathbf{g})\mathbf{F}_{\mathbf{g}'} = \mathbf{F}_{\mathbf{g}'}$ ,  $Q(\mathbf{g})\mathbf{F}_0 = \mathbf{F}_0$ , and Eq. (19b) becomes

$$F_{\mathbf{g}} = \rho\chi \left[ M(\mathbf{g})F_0 + \sum_{\mathbf{g}' \neq 0} M(\mathbf{g} - \mathbf{g}')F_{\mathbf{g}'} \right], \quad \mathbf{g} \neq 0. \quad (28)$$

The solution to this equation is

$$F_{\mathbf{g}} = \frac{\rho\chi}{1 - (1 - \rho)\chi} M(\mathbf{g})F_0, \quad (29)$$

where some of the properties (A.2) have been used (keeping in mind that the term  $\mathbf{g} = 0$  must be excluded from the summation). We then have

$$\Sigma_{zz} = \frac{\rho\chi}{1 - (1 - \rho)\chi} \sum_{\mathbf{g} \neq 0} M(-\mathbf{g})M(\mathbf{g}) = \frac{(1 - \rho)\chi}{1 - (1 - \rho)\chi}. \quad (30)$$

It can be seen from the above equation that  $\Sigma_{zz}$  does not approach zero when  $\rho \rightarrow 0$ , as was discussed in Sec. 3.3. Upon substitution of (30) into (23), we find that

$$\epsilon_{zz}^{\text{eff}} = (1 - \rho)\epsilon_b + \rho\epsilon_a = \langle \epsilon \rangle. \quad (31)$$

Thus, the effective permittivity for  $z$ -polarization is given by the arithmetic average of  $\epsilon(x, y)$ . This is in agreement with Krokhnin *al.* [20, 21].

### 3.5. Concept of the smooth field

The result (31) for a  $z$ -polarized wave could have been anticipated. To understand better why the effective permittivity in this case is given by an arithmetic average, it is instructive to consider the concept of the *smooth field*. The smooth field  $\mathbf{S}(\mathbf{r})$  changes slowly on the characteristic scale defined by the heterogeneities in the medium. As a result, one can factorize spatial averages of  $\mathbf{S}(\mathbf{r})$  multiplied by any rapidly-varying function. For example, we can write  $\langle \mathbf{S}\epsilon \rangle = \langle \mathbf{S} \rangle \langle \epsilon \rangle$ , etc.

Let us recall some well-known results for 1D periodically-layered media [23]. The effective permittivity of such media is  $\epsilon_{\parallel}^{\text{eff}} = \langle \epsilon \rangle$  for waves polarized parallel to the layers and  $\epsilon_{\perp}^{\text{eff}} = \langle \epsilon^{-1} \rangle^{-1}$  for waves polarized perpendicularly to the layers. These two results can be obtained quite expeditiously by applying the concept of the smooth field. In the case of tangential polarization, the electric field  $\mathbf{E}$  is smooth. This follows from the boundary condition which requires that the tangential components of the electric field be continuous at all interfaces. Consequently, we can write

$$\langle \mathbf{D} \rangle = \langle \epsilon \mathbf{E} \rangle = \langle \epsilon \rangle \langle \mathbf{E} \rangle , \quad (32)$$

from which it follows that  $\epsilon_{\parallel}^{\text{eff}} = \langle \epsilon \rangle$ . For perpendicular polarization, the field  $\mathbf{D}$  is smooth. We then write

$$\langle \mathbf{E} \rangle = \langle \epsilon^{-1} \mathbf{D} \rangle = \langle \epsilon^{-1} \rangle \langle \mathbf{D} \rangle \quad (33)$$

and  $\epsilon_{\perp}^{\text{eff}} = \langle \epsilon^{-1} \rangle^{-1}$ .

Similar considerations can be applied to the 2D problem of Sec. 3.4. For waves polarized along the  $z$ -axis, the field  $\mathbf{E}$  is smooth, which results in  $\epsilon_{zz}^{\text{eff}} = \langle \epsilon \rangle$ , in agreement with (31).

One can also consider a more general smooth field of the form  $\mathbf{S} = p\mathbf{E} + (1-p)\mathbf{D} = [p + (1-p)\epsilon]\mathbf{E}$ , where  $p$  is a mixing parameter. Here we consider the 3D case and assume that  $\mathbf{S}$  is smooth for any polarization state. Application of the smooth field principle results in the following equalities:

$$\langle \mathbf{E} \rangle = \langle \mathbf{S} \rangle \langle 1/[p + (1-p)\epsilon] \rangle , \quad \langle \mathbf{D} \rangle = \langle \mathbf{S} \rangle \langle \epsilon/[p + (1-p)\epsilon] \rangle , \quad (34)$$

from which we find the effective permittivity to be

$$\epsilon_{\alpha\beta}^{\text{eff}} = \delta_{\alpha\beta} \frac{\langle \epsilon/[\epsilon + p/(1-p)] \rangle}{\langle 1/[\epsilon + p/(1-p)] \rangle} . \quad (35)$$

Eq. (35) is, in fact, the Maxwell-Garnett formula. Although this form is rarely used, the Maxwell-Garnett effective permittivity can be written as

$$\epsilon_{\text{MG}} = \frac{\langle \epsilon/(\epsilon + 2\epsilon_b) \rangle}{\langle 1/(\epsilon + 2\epsilon_b) \rangle} . \quad (36)$$

We see that (35) and (36) coincide if  $p = 2\epsilon_b/(\epsilon + 2\epsilon_b)$ .

Thus, the Maxwell-Garnett EMT assumes that the field  $\mathbf{S} = [(\epsilon + 2\epsilon_b)/(\epsilon + 2\epsilon_b)]\mathbf{E}$  is smooth. Since the mixing parameter  $p$  depends on the permittivity of the host medium, Eq. (36) is not invariant with respect to the substitution  $\epsilon_a \leftrightarrow \epsilon_b$  and  $\rho \leftrightarrow 1 - \rho$ . The homogenization formula derived in this paper, however, is fully symmetric. Note that Bruggeman's EMT is also symmetric but can not be easily written in terms of averages. Therefore, it is not clear which form of the smooth field Bruggeman's approximation assumes. In general, the smooth field does not need to be a linear functional of  $\mathbf{E}$  and  $\mathbf{D}$ .

#### 4. Reflection and refraction at a half-space boundary

An infinite lattice is a mathematical abstraction. All experimental media are bounded, and the physical effects which occur at the boundary are often important. For instance, as mentioned above, it is not possible to determine simultaneously the effective permittivity and permeability of a medium from the bulk dispersion relation alone.

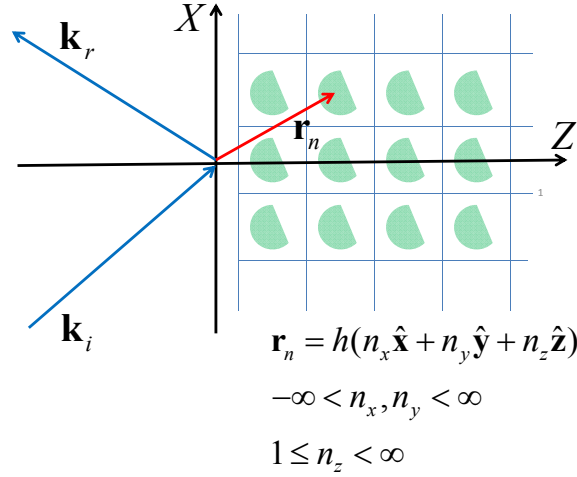


**Figure 2.** (color online) Sketch of the geometry considered: reflection and refraction at a half-space boundary.

The problem of reflection and refraction of a wave at a flat interface is considered in this section. The goals are three-fold. First, we will derive the limit in which the correct expression for the Fresnel reflection coefficient is obtained. This will turn out to be the same limit as was used in Sec. 3.1. Second, we will show that the correct expression for the reflection coefficients results only if we set  $\mu^{\text{eff}} = 1$ . Third, we will provide additional mathematical justification for the results of Sec. 3.1. Indeed, the derivations of that section contain one dubious step. Namely, the applicability of the Poisson summation formula (14) can be questioned because the variable  $\mathbf{q}$  is complex. Strictly speaking, the series in the left-hand side of (14) diverges for an infinite lattice. The problem can be fixed, in principle, by considering real-valued  $\mathbf{q}$ 's and then analytically-continuing the summation result to the whole complex plane. In this section, no such complication will arise since all series in question are convergent.

#### 4.1. General setup

The geometry considered in this section is sketched in Fig. 2. The medium occupies the right half-space and the left half-space has the background permittivity  $\epsilon_b$ . It would be more appropriate to consider the case when the left half-space is vacuum and the right half-space is a two-component mixture, so that there are three different components in the problem. This, however, requires the use of the half-space Green's tensor [24] – a step that is not conceptually difficult, yet is mathematically involved. Here we restrict consideration to two components. This includes the cases when the host medium is vacuum and also when the incident beam is first refracted from vacuum into a homogeneous medium of permittivity  $\epsilon_b \neq 1$  (at a planar interface that is located at  $z = z_1 \ll -h$  and is not considered explicitly) and then into a heterogeneous medium which is a mixture of  $a$ - and  $b$ -type components.

Physically, the  $z$ -coordinate of the effective medium boundary can be stated only

approximately, within an interval of width  $\sim h$ . It will prove mathematically convenient to place the boundary on the plane  $z = 0$ , and the centers of the left-most cells on the plane  $z = h$ , as shown in Fig. 2. In the EMT developed below, the half-space  $z > 0$  is assumed to be filled with an effective medium.

A wave can not propagate in a semi-infinite medium without an external source. Therefore, we must solve the integral equation (2) with a nonzero incident field  $\mathbf{E}_i$  which we will take to be a plane wave. We will also find that, under appropriate conditions, a uniquely-defined reflected plane wave  $\mathbf{E}_r$  exists in the region  $z < 0$ . The incident and the reflected waves are given by

$$\mathbf{E}_i(\mathbf{r}) = \mathbf{A}_i \exp(\mathbf{k}_i \cdot \mathbf{r}) , \quad -\infty < z < \infty , \quad (37a)$$

$$\mathbf{E}_r(\mathbf{r}) = \mathbf{A}_r \exp(\mathbf{k}_r \cdot \mathbf{r}) , \quad -\infty < z < 0 . \quad (37b)$$

Note that the incident wave is defined in the whole space but Eq. (2) is only defined for  $\mathbf{r} \in \Omega_{\text{tot}}$ . The wave numbers of the incident and the reflected waves can be written as

$$\mathbf{k}_i = \mathbf{k}_\perp + \hat{\mathbf{z}}k_{iz} , \quad \mathbf{k}_r = \mathbf{k}_\perp - \hat{\mathbf{z}}k_{iz} . \quad (38)$$

Henceforth, the subscript “ $\perp$ ” will be used to denote projections of vectors onto the  $xy$ -plane. Note that  $\mathbf{k}_\perp \cdot \hat{\mathbf{z}} = 0$  and

$$k_i^2 = k_r^2 = k_\perp^2 + k_{iz}^2 = k_0^2 = (\omega/c)^2 \epsilon_b . \quad (39)$$

It is important to note that the vector  $\mathbf{k}_\perp$  is purely real. A complex-valued  $\mathbf{k}_\perp$  would imply a wave that is evanescent in a direction parallel to the interface. This would necessitate the presence of additional interfaces; such a possibility is not considered here. The vector  $\mathbf{k}_\perp$  is real-valued even if the host medium is absorbing. Indeed, we should keep in mind that the incident wave enters the host medium from vacuum and that the tangential component of the wave vector is conserved at any planar interface, even if one of the media is absorbing. However, the  $z$ -projection of  $\mathbf{k}_i$  does not need to be real. In a transparent host ( $k_0 > 0$ ), the incident wave is evanescent and  $k_{iz}$  is purely imaginary if  $k_\perp > k_0$ ; in an absorbing host,  $k_{iz}$  is, generally, complex.

Note that the reflected wave (37b) does not enter Eq. (2) because it is identically zero in  $\Omega_{\text{tot}}$ . The reflected wave is computed *a posteriori* once the polarization field  $\mathbf{P}$  is found. Then the amplitudes  $\mathbf{A}_r$  and  $\mathbf{A}_i$  can be used to determine the reflection coefficient.

To solve Eq. (2) in the presence of the incident field, we decompose  $\mathbf{P}$  as

$$\mathbf{P} = \mathbf{P}_B + \mathbf{P}_S , \quad (40)$$

where  $\mathbf{P}_B$  is the Bloch wave of the form (8) and  $\mathbf{P}_S$  is an additional wave that originates due to the presence of the surface. We seek the condition under which



$$\mathbf{E}_{\text{EO}}(\mathbf{r}) \equiv \int_{\Omega_{\text{tot}}} G(\mathbf{r}, \mathbf{r}') \mathbf{P}_B(\mathbf{r}') d^3 r' = \mathbf{E}_B(\mathbf{r}) + \mathbf{E}_{\text{ext}}(\mathbf{r}) + \mathbf{E}_S(\mathbf{r}) , \quad (41)$$

where in  $\Omega_{\text{tot}}$

$$\frac{3\chi}{4\pi} \mathbf{E}_B = \mathbf{P}_B , \quad (42a)$$

$$-\mathbf{E}_{\text{ext}} = \mathbf{E}_i , \quad (42b)$$

and  $\mathbf{E}_S$  decays exponentially away from the interface. If (40)-(42) hold, then Eq. (2) becomes

$$\mathbf{P}_S(\mathbf{r}) = \frac{3\chi}{4\pi} \left[ \mathbf{E}_S(\mathbf{r}) + \int_{\Omega_{\text{tot}}} G(\mathbf{r}, \mathbf{r}') \mathbf{P}_S(\mathbf{r}') d^3 r' \right] , \quad \mathbf{r} \in \Omega_{\text{tot}} . \quad (43)$$

Note that Eq. (43) contains only quantities which are associated with the surface wave.

Eq. (41) is the mathematical formulation of the Ewald-Oseen extinction theorem and we will refer to  $\mathbf{E}_{\text{EO}}$  as to the Ewald-Oseen field. We will see that one can determine the reflection coefficient from the conditions (42). We will also see that the surface wave is exponentially localized near the interface and does not contribute to either reflection or transmission coefficients if

$$(\mathbf{k}_{\perp} + \mathbf{g}_{\perp})^2 > k_0^2 , \quad \mathbf{g}_{\perp} \neq 0 . \quad (44)$$

Inequality (44) is weaker than what is required for homogenization. It is merely the condition that there is no Bragg diffraction in the medium; if (44) is violated, the conventional reflection and transmission coefficients can not be defined. If, however, (44) holds, we do not need to solve Eq. (43) explicitly; it suffices to know that the surface wave does not contribute to any measurement performed sufficiently far from the interface.

#### 4.2. Evaluation of the Ewald-Oseen field

To compute the Ewald-Oseen field, we proceed along the lines of Sec. 3.1 to arrive at the following expression:

$$\mathbf{E}_{\text{EO}}(\mathbf{r}) = \frac{4\pi}{3} \int \frac{d^3 p}{(2\pi)^3} K(\mathbf{p}) \int_{\Omega} d^3 R \mathbf{F}(\mathbf{R}) \exp [i\mathbf{p} \cdot (\mathbf{r} - \mathbf{R})] \sum_m \exp [i(\mathbf{q} - \mathbf{p}) \cdot \mathbf{r}_m] . \quad (45)$$

So far, no restrictions on  $\mathbf{r}$  have been placed. In particular,  $\mathbf{r}$  can be either in the right or left half-space. However, when we later substitute the result of integration into Eqs. (42),  $\mathbf{r}$  will be restricted to  $\Omega_{\text{tot}}$ .

The sum over  $m$  in (45) can be evaluated as follows. First, we expand the summation as



$$\sum_m \exp [i(\mathbf{q} - \mathbf{p}) \cdot \mathbf{r}_m] = \sum_{m_x, m_y = -\infty}^{\infty} \exp [i(q_x - p_x)hm_x + i(q_y - p_y)hm_y] \sum_{m_z=1}^{\infty} \exp [i(q_z - p_z)hm_z] . \quad (46)$$

From symmetry considerations, we know that  $\mathbf{q}_\perp = \mathbf{k}_\perp$ . This property is a manifestation of momentum conservation and will be confirmed below by considering the conditions (42). Since, as discussed above,  $\mathbf{k}_\perp$  is purely real,  $q_x$  and  $q_y$  are also real. Therefore, we can compute the sums over  $m_x$  and  $m_y$  using the Poisson sum formula. Further, the half-range sum over  $m_z$  converges absolutely because the transmitted wave decays into the medium and, correspondingly,  $\text{Im}q_z > 0$ . We, therefore, have

$$\sum_m \exp [i(\mathbf{q} - \mathbf{p}) \cdot \mathbf{r}_m] = \left(\frac{2\pi}{h}\right)^2 f(p_z) \sum_{\mathbf{g}_\perp} \delta(\mathbf{p}_\perp - \mathbf{q}_\perp - \mathbf{g}_\perp) , \quad (47)$$

where

$$f(p_z) \equiv \sum_{m_z=1}^{\infty} \exp [i(q_z - p_z)hm_z] = \frac{1}{\exp[i(p_z - q_z)h] - 1} \quad (48a)$$

$$= \frac{2\pi}{h} \sum_{g_z} \frac{(2\pi i)^{-1}}{p_z - q_z - g_z} . \quad (48b)$$

Here the well-known Laurant expansion of the function  $1/[\exp(iz) - 1]$  has been used. The equality (48b) is an important observation. It will allow us to evaluate the Ewald-Oseen field.

We now proceed by substituting (47) into (45), which yields

$$\begin{aligned} \mathbf{E}_{\text{EO}}(\mathbf{r}) &= \frac{4\pi}{3h^2} \sum_{\mathbf{g}_\perp} \int_{-\infty}^{\infty} \frac{dp_z}{2\pi} f(p_z) K(\mathbf{q}_\perp + \mathbf{g}_\perp + \hat{\mathbf{z}}p_z) \\ &\times \int_{\Omega} d^3\mathbf{R} \mathbf{F}(\mathbf{R}) \exp [i(\mathbf{q}_\perp + \mathbf{g}_\perp + \hat{\mathbf{z}}p_z) \cdot (\mathbf{r} - \mathbf{R})] . \end{aligned} \quad (49)$$

The integral over  $p_z$  can be computed by contour integration since all the poles and residues of the integrand are known. The positions of the poles in the complex  $p_z$ -plane are shown in Fig. 3. The poles at  $p_z = q_z + g_z$  are the singularities of the function  $f(p_z)$ . Since  $q_z$  has a positive imaginary part and all  $g_z$ 's are real-valued, these poles lie in the upper half-plane. The remaining poles are the singularities of  $K(\mathbf{q}_\perp + \mathbf{g}_\perp + \hat{\mathbf{z}}p_z)$  which is viewed here as a function of  $p_z$ . From the definition (6), we find that these singularities are located at  $p_z = \pm \mathcal{P}_{\mathbf{g}_\perp}$ , where

$$\mathcal{P}_{\mathbf{g}_\perp} = \sqrt{k_0^2 - (\mathbf{q}_\perp + \mathbf{g}_\perp)^2} . \quad (50)$$

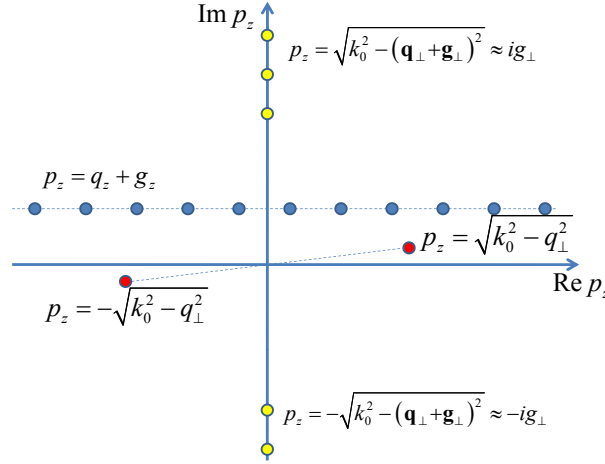


**Figure 3.** (color online) Poles of the integrand of Eq. (49) in the complex  $p_z$ -plane.

These poles can be considered separately for  $\mathbf{g}_\perp = 0$  and  $\mathbf{g}_\perp \neq 0$ . The two poles corresponding to  $\mathbf{g}_\perp = 0$  are  $p_z = \pm \mathcal{P}_0 = \pm \sqrt{k_0^2 - q_\perp^2}$ . The poles with  $\mathbf{g}_\perp \neq 0$  have large (either positive or negative) imaginary parts if  $hk_0, hq_\perp \ll 1$ , in which case they can be written, approximately, as  $\mathcal{P}_{\mathbf{g}_\perp} \approx i\mathbf{g}_\perp$ .

Note that in the case of infinite lattices, the singularities of  $K(\mathbf{p})$  do not contribute to Fourier integrals of the type (12) because the corresponding residues are identically zero (these singularities fall in between the peaks of the delta-function fence given by the right-hand side of (14)).

We will compute the contributions of the different families of poles to the integral (49) separately. If the vector of position  $\mathbf{r}$  is inside one of the inclusions, the integration contour must be closed in the upper half of the complex  $p_z$ -plane. Correspondingly, only the poles with positive imaginary parts contribute to the integral (49) in this case. The Ewald-Oseen field can also be computed in the left half-space. If the point of observation  $\mathbf{r}$  is further away from the interface than  $h/2$ , so that the inequality  $\hat{\mathbf{z}} \cdot \mathbf{r} < -h/2$  holds, the integration contour must be closed in the lower half of the complex  $p_z$  plane. In what follows, it will be shown that the poles at  $p_z = q_z + g_z$  yield the Bloch-wave field  $\mathbf{E}_B(\mathbf{r})$ , the pole at  $p_z = \mathcal{P}_0$  yields the extinction field  $\mathbf{E}_{\text{ext}}(\mathbf{r})$ , the pole at  $p_z = -\mathcal{P}_0$  yields the reflected wave, and, finally, the poles  $p_z \approx \pm \mathcal{P}_{\mathbf{g}_\perp}$  with  $\mathbf{g}_\perp \neq 0$  yield the fast-decaying surface wave.

**4.2.1. Bloch wave.** We start by computing the Bloch-wave contribution to the Ewald-Oseen field,  $\mathbf{E}_B(\mathbf{r})$ . We place the point of observation in  $\Omega_{\text{tot}}$ , use the expression (48b) for  $f(p_z)$  and evaluate the contributions of the poles  $p_z = q_z + g_z$  to the integral (49). This results in the following expression:

$$\mathbf{E}_B(\mathbf{r}) = \frac{4\pi}{3h^3} \sum_{\mathbf{g}} \exp[i(\mathbf{q} + \mathbf{g}) \cdot \mathbf{r}] K(\mathbf{q} + \mathbf{g}) \int_{\Omega} \mathbf{F}(\mathbf{R}) \exp[-i(\mathbf{q} + \mathbf{g}) \cdot \mathbf{R}] d^3R, \quad (51)$$

$$\mathbf{r} \in \Omega_{\text{tot}}.$$

Here we have used the equalities  $\mathbf{g}_{\perp} + \hat{\mathbf{z}}g_z = \mathbf{g}$  and  $\sum_{\mathbf{g}_{\perp}} \sum_{g_z} = \sum_{\mathbf{g}}$ . Now, if  $\mathbf{F}(\mathbf{R})$  is expanded according to (16), and if the expansion coefficients  $\mathbf{F}_{\mathbf{g}}$  satisfy (17), then the field given by Eq. (51) satisfies  $\mathbf{E}_B(\mathbf{r}) = (4\pi/3\chi)\mathbf{P}_B(\mathbf{r})$  for  $\mathbf{r} \in \Omega_{\text{ot}}$ , where  $\mathbf{P}_B$  is of the form (8). Thus, (42a) is satisfied if the Bloch wave of the polarization  $\mathbf{P}_B$  is the same as one would find by solving the eigenproblem (17) for an infinite medium. This justifies the use of the Poisson summation formula in Sec. 3.1.

Eq. (17) applies to general photonic crystals that are not necessarily describable by effective medium parameters. As was discussed in Sec. 3.1, homogenization is obtained by taking the limit  $h \rightarrow 0$ . This limit must be computed separately for the equations with  $\mathbf{g} = 0$  and  $\mathbf{g} \neq 0$ , which results in (19). This system of equations defines an eigenproblem for the Bloch wave vector  $\mathbf{q}$ , while the polarization vector  $\mathbf{F}_0$  is obtained as an eigenvector of (21). The higher-order expansion coefficients  $\mathbf{F}_{\mathbf{g}}$  are uniquely determined by  $\mathbf{F}_0$  but  $\mathbf{F}_0$  itself is defined by (19) only up to a multiplicative factor. Next, we will show that this factor is fixed by the condition (42b).

*4.2.2. Extinction wave.* We now compute the contribution of the pole located at  $p_z = \mathcal{P}_0$ . The function  $f(p_z)$  is analytic in the vicinity of  $\mathcal{P}_0$ ; therefore, we can use the expression (48a) for  $f(p_z)$ . Since Eqs. (42b) should hold only for  $\mathbf{r} \in \Omega_{\text{tot}}$ , we close the integration contour in the upper half-plane. A straightforward calculation yields

$$\begin{aligned} \mathbf{E}_{\text{ext}}(\mathbf{r}) = & \frac{4\pi i k_0^2 - (\mathbf{q}_{\perp} + \hat{\mathbf{z}}\mathcal{P}_0) \otimes (\mathbf{q}_{\perp} + \hat{\mathbf{z}}\mathcal{P}_0)}{h^2 2\mathcal{P}_0} \frac{\exp[i(\mathbf{q}_{\perp} + \hat{\mathbf{z}}\mathcal{P}_0) \cdot \mathbf{r}]}{\exp[i(\mathcal{P}_0 - q_z)h] - 1} \\ & \times \int_{\Omega} d^3R \mathbf{F}(\mathbf{R}) \exp[-i(\mathbf{q}_{\perp} + \hat{\mathbf{z}}\mathcal{P}_0) \cdot \mathbf{R}], \quad \mathbf{r} \in \Omega_{\text{tot}}. \end{aligned} \quad (52)$$

We seek the condition under which  $\mathbf{E}_{\text{ext}}(\mathbf{r}) = -\mathbf{E}_i(\mathbf{r})$  for  $\mathbf{r} \in \Omega_{\text{tot}}$ , where  $\mathbf{E}_i(\mathbf{r})$  is given by (37a). It immediately transpires that the above equality can hold only if  $\mathbf{q}_{\perp} = \mathbf{k}_{\perp}$ . The continuity of the tangential components of all wave vectors, including the incident wave vector  $\mathbf{k}_i$ , the reflected wave vector  $\mathbf{k}_r$  and the Bloch wave vector of the transmitted wave  $\mathbf{q}$  follows from the discrete translational symmetry of the problem. We now find from (38) that  $\mathcal{P}_0 = k_{iz}$  and  $\mathbf{q}_{\perp} + \hat{\mathbf{z}}\mathcal{P}_0 = \mathbf{k}_i$ . With the use of these equalities and the notation

$$\tilde{\mathbf{F}}(\mathbf{k}) = \int_{\Omega} \mathbf{F}(\mathbf{R}) \exp(-i\mathbf{k} \cdot \mathbf{R}) d^3R, \quad (53)$$

we can simplify Eq. (52) as

$$\mathbf{E}_{\text{ext}}(\mathbf{r}) = \frac{4\pi i}{h^2} \frac{k_0^2 - \mathbf{k}_i \otimes \mathbf{k}_i}{2k_{iz}} \frac{\exp[i\mathbf{k}_i \cdot \mathbf{r}]}{\exp[i(k_{iz} - q_z)h] - 1} \tilde{\mathbf{F}}(\mathbf{k}_i), \quad \mathbf{r} \in \Omega_{\text{tot}}. \quad (54)$$

The extinction condition then takes the form

$$\mathbf{A}_i = -\frac{2\pi i}{h^2} \frac{k_0^2 - \mathbf{k}_i \otimes \mathbf{k}_i}{\exp[i(k_{iz} - q_z)h] - 1} \frac{\tilde{\mathbf{F}}(\mathbf{k}_i)}{k_{iz}}. \quad (55)$$

So far, no approximations have been made. The homogenization limit is obtained by observing that

$$\lim_{h \rightarrow 0} \left\{ \exp[i(\pm k_{iz} - q_z)h] - 1 \right\} = i(\pm k_{iz} - q_z)h, \quad (56a)$$

$$\lim_{h \rightarrow 0} \tilde{\mathbf{F}}(\mathbf{k}_i) = \lim_{h \rightarrow 0} \tilde{\mathbf{F}}(\mathbf{k}_r) = V(1 + \Sigma)\mathbf{F}_0. \quad (56b)$$

Once the above limiting expressions are used, the extinction condition becomes of the form

$$\mathbf{A}_i = -2\pi\rho \frac{k_0^2 - \mathbf{k}_i \otimes \mathbf{k}_i}{k_{iz}(k_{iz} - q_z)} (1 + \Sigma)\mathbf{F}_0. \quad (57)$$

This equation couples the amplitude of the incident field,  $\mathbf{A}_i$ , and the amplitude of the Bloch polarization wave,  $\mathbf{F}_0$ . The vector  $\mathbf{F}_0$  must simultaneously satisfy the following two conditions: (i) be an eigenvector of the tensor in the square brackets in Eq. (21) and (ii) satisfy (57). These two conditions determine both the direction and the length of  $\mathbf{F}_0$ .

*4.2.3. Reflected wave.* Consider now the case when the point of observation  $\mathbf{r}$  in the left half-space. As discussed above, we will place  $\mathbf{r}$  at least  $h/2$  away from the interface. This will allow us to close the integration contour in (49) in the lower half of the complex  $p_z$ -plane. The reflected wave is obtained by computing the input of the pole  $p_z = -\mathcal{P}_0$ . We find that the electric field of the reflected wave is of the form (37b) where the amplitude  $\mathbf{A}_r$  is given by

$$\mathbf{A}_r = \frac{2\pi i}{h^2} \frac{k_0^2 - \mathbf{k}_r \otimes \mathbf{k}_r}{\exp[-i(k_{iz} + q_z)h] - 1} \frac{\tilde{\mathbf{F}}(\mathbf{k}_r)}{k_{iz}}. \quad (58)$$

This expression contains no approximations. In the homogenization limit, we use the limiting expressions (56) and obtain

$$\mathbf{A}_r = -2\pi\rho \frac{k_0^2 - \mathbf{k}_r \otimes \mathbf{k}_r}{k_{iz}(k_{iz} + q_z)} (1 + \Sigma)\mathbf{F}_0. \quad (59)$$

4.2.4. *Surface wave.* Finally, let us evaluate the contribution of the poles  $p_z = \mathcal{P}_{\mathbf{g}_\perp}$  with  $\mathbf{g}_\perp \neq 0$ . For  $\mathbf{r} \in \Omega_{\text{tot}}$ , we have

$$\mathbf{E}_S(\mathbf{r}) = \frac{2\pi i}{h^2} \sum_{\mathbf{g}_\perp \neq 0} f(\mathcal{P}_{\mathbf{g}_\perp}) \frac{k_0^2 - \mathbf{k}_{\mathbf{g}_\perp} \otimes \mathbf{k}_{\mathbf{g}_\perp}}{\mathcal{P}_{\mathbf{g}_\perp}} \exp(i\mathbf{k}_{\mathbf{g}_\perp} \cdot \mathbf{r}) \tilde{\mathbf{F}}(\mathbf{k}_{\mathbf{g}_\perp}) , \quad \mathbf{r} \in \Omega_{\text{tot}} \quad (60)$$

where

$$\mathbf{k}_{\mathbf{g}_\perp} = \mathbf{q}_\perp + \mathbf{g}_\perp + \hat{\mathbf{z}}\mathcal{P}_{\mathbf{g}_\perp} . \quad (61)$$

If the condition (44) holds, the quantities  $\mathcal{P}_{\mathbf{g}_\perp}$  have nonzero imaginary parts even if the host is transparent. Therefore, the surface wave decays exponentially away from the interface. In the homogenization limit, the exponential decay is fast. Indeed, in the limit  $h \rightarrow 0$ , we have (for  $\mathbf{g}_\perp \neq 0$ ):  $\mathcal{P}_{\mathbf{g}_\perp} \rightarrow ig_\perp$ ,  $\mathbf{k}_{\mathbf{g}_\perp} \rightarrow \mathbf{g}_\perp + i\hat{\mathbf{z}}g_\perp$ ,  $f(\mathcal{P}_{\mathbf{g}_\perp}) \rightarrow -1/g_\perp h$ . With these limits taken into account, the surface wave takes the following form:

$$\begin{aligned} \mathbf{E}_S(\mathbf{r}) = & -\frac{2\pi i}{h^3} \sum_{\mathbf{g}_\perp \neq 0} \frac{k_0^2 - (\mathbf{g}_\perp + i\hat{\mathbf{z}}g_\perp) \otimes (\mathbf{g}_\perp + i\hat{\mathbf{z}}g_\perp)}{g_\perp^2} \\ & \times \exp[(i\mathbf{g}_\perp - \hat{\mathbf{z}}g_\perp) \cdot \mathbf{r}] \tilde{\mathbf{F}}(\mathbf{g}_\perp + \hat{\mathbf{z}}g_\perp) , \quad \mathbf{r} \in \Omega_{\text{tot}} . \end{aligned} \quad (62)$$

It can be seen that  $\mathbf{E}_S$  decays exponentially on the scale of  $h$ . So does the wave of polarization  $\mathbf{P}_S$ , as both fields are related by the integral equation (43).

Solving Eq. (43) numerically can be a very difficult task. Fortunately, doing so is not necessary if one is only concerned with far-field measurements.

### 4.3. Reflection coefficient

We will now utilize the results of the previous subsection to compute the reflection coefficients for the half-space. We will use the assumption of Sec. 3.2, namely, that the crystallographic and optical axes of the medium coincide so that the tensor  $\Sigma$  is diagonal in the laboratory frame. Apart from other simplifications, media of this type are nonchiral and do not rotate the polarization of the transmitted and reflected waves. This property holds even beyond the homogenization limit, since it is a straightforward consequence of the elementary cell symmetries, and it will enable us to consider the s- and p-polarizations separately.

In this subsection, we will explicitly use the reference frame shown in Fig. 2. That is, we will assume that the plane of incidence is the  $xz$ -plane and that the projection of the wave vectors  $\mathbf{k}_i$ ,  $\mathbf{k}_r$  and  $\mathbf{q}$  onto the interface is  $\mathbf{k}_\perp = k_x \hat{\mathbf{x}}$ .

4.3.1. *S-polarization.* In the case of s-polarization, the incident and reflected waves are polarized perpendicularly to the plane of incidence. Consequently, we have  $\mathbf{A}_i, \mathbf{A}_r \propto \hat{\mathbf{y}}$ , and the reflection coefficient is given by

$$r = \frac{\mathbf{A}_r \cdot \hat{\mathbf{y}}}{\mathbf{A}_i \cdot \hat{\mathbf{y}}} = - \frac{\tilde{\mathbf{F}}(\mathbf{k}_r) \cdot \hat{\mathbf{y}}}{\tilde{\mathbf{F}}(\mathbf{k}_i) \cdot \hat{\mathbf{y}}} \frac{\exp[i(k_{iz} - q_z)h] - 1}{\exp[-i(k_{iz} + q_z)h] - 1}. \quad (63)$$

This is an exact expression that retains its physical meaning as long as (44) holds. In the homogenization limit, we use the limiting expressions (56) to obtain

$$r = \frac{k_{iz} - q_z}{k_{iz} + q_z}. \quad (64)$$

Here  $q_z$  is determined by taking the square root of the right-hand side of (25a) where  $\epsilon_{xx}^{\text{eff}}, \epsilon_{zz}^{\text{eff}}$  are given by (23) and the branch of the square root is determined by the condition  $\text{Im}(q_z) > 0$ . The expression (64) should be compared to the corresponding Fresnel coefficient  $r_F$  for a homogeneous medium characterized by the permittivity and permeability tensors  $\epsilon^{\text{eff}}$  and  $\mu^{\text{eff}}$ :

$$r_F = \frac{k_{iz} - q_z/\mu_{xx}^{\text{eff}}}{k_{iz} + q_z/\mu_{xx}^{\text{eff}}}. \quad (65)$$

It can be seen that the two coefficients coincide only if we set  $\mu_{xx}^{\text{eff}} = 1$ . Since the medium can be illuminated from all three directions, one can conclude that  $\mu_{xx}^{\text{eff}} = \mu_{yy}^{\text{eff}} = \mu_{zz}^{\text{eff}} = 1$ , so that the whole tensor  $\mu^{\text{eff}}$  is equal to the identity operator. This justifies the choice  $\mu^{\text{eff}} = 1$  that was made in Sec. 3.1.

*4.3.2. P-polarization.* In the case of p-polarization, the reflection coefficient can be conveniently defined by using the ratio of tangential components of the magnetic field for the reflected and incident waves. The magnetic field amplitudes are given by  $k_0^{-1} \mathbf{k}_{i,r} \times \mathbf{A}_{i,r}$  and are aligned with the  $y$ -axis. Therefore, the exact reflection coefficient is given by

$$r = - \frac{[\mathbf{k}_r \times \tilde{\mathbf{F}}(\mathbf{k}_r)] \cdot \hat{\mathbf{y}}}{[\mathbf{k}_i \times \tilde{\mathbf{F}}(\mathbf{k}_i)] \cdot \hat{\mathbf{y}}} \frac{\exp[i(k_{iz} - q_z)h] - 1}{\exp[-i(k_{iz} + q_z)h] - 1}. \quad (66)$$

In the homogenization limit, this expression is simplified by using the limits (56), which leads to

$$r = - \frac{[\mathbf{k}_r \times (1 + \Sigma)\mathbf{F}_0] \cdot \hat{\mathbf{y}}}{[\mathbf{k}_i \times (1 + \Sigma)\mathbf{F}_0] \cdot \hat{\mathbf{y}}} \frac{k_{iz} - q_z}{k_{iz} + q_z}. \quad (67)$$

At this point, we use the dispersion relation (25a) for  $q_z$  and the ratio of the  $x$ - and  $z$ -components of the vector  $\mathbf{F}_0$  which is given in (26). It can be shown by a tedious but straightforward calculation that (67) is equivalent to the following expression:

$$r = \frac{k_{iz} - q_z/\epsilon_{xx}^{\text{eff}}}{k_{iz} + q_z/\epsilon_{xx}^{\text{eff}}}, \quad (68)$$

where  $q_z$  is determined as is explained in the text following Eq. (64) and  $\epsilon_{\alpha\alpha}^{\text{eff}}$  is given by (23).

The formula (68) coincides exactly with the Fresnel reflection coefficient for a p-polarized wave reflected from a half-space characterized by the permittivity tensor  $\epsilon^{\text{eff}}$  and permeability  $\mu^{\text{eff}} = 1$ . Thus, for both polarizations, the correct Fresnel reflection coefficients are obtained by setting  $\mu^{\text{eff}} = 1$  and using the expression (23).

## 5. Comparison of point-dipole and continuous-medium models

The model of point-like polarizable particles arranged on a three-dimensional infinite lattice possesses an intuitive physical appeal. Historically, many authors have used this model and, although an exhaustive review is outside of the scope of this paper, Refs. [14–16, 22, 25, 26] can be mentioned. Unfortunately, the model is haunted by divergences. In this section, we will discuss the nature and origins of these divergences and some of the commonly-used methods for their regularization. We will also attempt, to the degree it is possible, to establish a correspondence between the model of point dipoles and the model of a continuous two-component medium, which is the subject of this paper.

The model of point dipoles considers an array of point-like particles which have well-defined locations, but no shape or size. Instead of the latter two physical characteristics, the electric dipole polarizability  $\alpha$  is used. In some generalizations of the model, the magnetic dipole polarizability is also included. The basic idea of this approach is that the electromagnetic response of a particle is completely characterized by its polarizability.

If only the electric polarizability is retained, one arrives, in lieu of the integral equation (2), at the set of algebraic equations

$$\frac{1}{\alpha} \mathbf{d}_n = \mathbf{E}_i(\mathbf{r}_n) + \sum_{m \neq n} G(\mathbf{r}_n, \mathbf{r}_m) \mathbf{d}_m. \quad (69)$$

Here  $\mathbf{d}_n$  is the electric dipole moment of the  $n$ -th particle. Now two important points should be made. First, the summation on the right-hand side of (69) is restricted only to the indices  $m$  which are not equal to  $n$ . This reflects the idea that the electric field at the site of the  $n$ th dipole is a superposition of the incident wave  $\mathbf{E}_i(\mathbf{r}_n)$  and the waves scattered by all other dipoles. Second, energy conservation requires that [27–29]  $\text{Im}(1/\alpha) \leq -2k_0^3/3$ . If the equality holds, the particles are non-absorbing. It is convenient to decompose the inverse polarizability as

$$\frac{1}{\alpha} = \frac{1}{\alpha_{\text{LL}}} - i \frac{2k_0^3}{3}, \quad (70)$$

where  $\alpha_{\text{LL}}$  is the “Lorenz-Lorentz” quasistatic polarizability and  $-i2k_0^3/3$  is the first non-vanishing radiative correction to the imaginary part of  $1/\alpha$ . Radiative corrections to the real part of  $1/\alpha$  also exist and are, in fact, of a lower order in  $k_0$ , but it is the correction to the imaginary part which is physically important and should be retained even in the limit  $k_0 h \rightarrow 0$ . We will see momentarily that the two seemingly unrelated facts mentioned above are mathematically connected.

We now consider an infinite lattice, set the incident field to zero and seek the solution to (69) in the form  $\mathbf{d}_n = \mathbf{d} \exp(i\mathbf{q} \cdot \mathbf{r}_n)$ . This results in the eigenproblem

$$\frac{1}{\alpha} \mathbf{d} = S(\mathbf{q}) \mathbf{d} , \quad (71)$$

where

$$S(\mathbf{q}) = \sum_{m \neq n} G(\mathbf{r}_n, \mathbf{r}_m) \exp[-i\mathbf{q} \cdot (\mathbf{r}_n - \mathbf{r}_m)] \quad (72)$$

is the dipole sum. Using the Fourier representation (5), we rewrite (72) as

$$S(\mathbf{q}) = \frac{4\pi}{3} \int \frac{d^3p}{(2\pi)^3} K(\mathbf{p}) \sum_{m \neq n} \exp[i(\mathbf{p} - \mathbf{q}) \cdot (\mathbf{r}_m - \mathbf{r}_n)] . \quad (73)$$

The first complication encountered in the above is that the summation on the right-hand side of (73) is incomplete. We can easily fix this problem by adding and subtracting unity to the series, which leads to

$$S(\mathbf{q}) = \frac{4\pi}{3} \left[ \frac{1}{h^3} \sum_{\mathbf{g}} K(\mathbf{q} + \mathbf{g}) - \int \frac{d^3p}{(2\pi)^3} K(\mathbf{p}) \right] , \quad (74)$$

where we have used the Poisson summation formula (14). Still, both terms on the right-hand side of (74) are divergent. We will deal with the integral first. To this end, we utilize the expression for  $K(\mathbf{p})$  given in (6) and notice that the angular integral of the term  $p^2 - 3\mathbf{p} \otimes \mathbf{p}$  is zero in three dimensions. Therefore, we have

$$I \equiv \int \frac{d^3p}{(2\pi)^3} K(\mathbf{p}) = 4\pi \int_0^\infty \frac{p^2 dp}{(2\pi)^3} \frac{2k_0^2}{p^2 - k_0^2} . \quad (75)$$

This is still a divergent integral. We can regularize (75) by writing

$$I = \lim_{\xi \rightarrow 0} \left\{ 4\pi \int_0^\infty \frac{p^2 dp}{(2\pi)^3} \frac{2k_0^2}{p^2 - k_0^2} \exp[-(\xi p)^2] \right\} . \quad (76)$$

The above limit indeed exists and is equal to  $ik_0^3/2\pi$ , assuming that  $\text{Im}k_0 > 0$  (we take  $k_0 = \omega/c + i0$  in vacuum). Upon substitution of this result into (74), we find that

$$\frac{4\pi}{3} \left[ - \int \frac{d^3p}{(2\pi)^3} K(\mathbf{p}) \right] = -i \frac{2k_0^3}{3} . \quad (77)$$

We now use the decomposition (70) and notice that the above term is canceled by a similar term on the left-hand side of (71). Taking into account this cancellation, (71) becomes

$$\frac{1}{\alpha_{\text{LL}}} \mathbf{d} = \frac{4\pi}{3h^3} \sum_{\mathbf{g}} K(\mathbf{q} + \mathbf{g}) \mathbf{d} . \quad (78)$$



The mathematical tricks used so far are not very objectionable. The result (77) is a reflection of the fact that

$$\lim_{\xi \rightarrow 0} \left[ \frac{3}{4\pi\xi^3} \int_{|\mathbf{r}' - \mathbf{r}| \leq \xi} G(\mathbf{r}, \mathbf{r}') d^3r' \right] = -i \frac{2k_0^3}{3} . \quad (79)$$

Here we have assumed that the particle is spherically symmetric. The use of a different integration volume in (79), or of a different regularization function in (76), would certainly yield a different result. Fortunately, if  $k_0 h \ll 1$ , only the real part of  $I$  is affected by the choice of the regularization function in (76) while the imaginary part is relatively stable. If  $\text{Re}I$  is unimportant (e.g., it is small compared to the sum of real parts all other contributions in (74)), then (78) is a good approximation regardless of the true shape of the particles.

However, the divergence of the series in the right-hand side of (78) is truly problematic. One can attempt to regularize this divergence by the same mathematical trick that was used above. However, the result of such a manipulation would indeed depend on the regularization function in a nontrivial way. One can conclude that knowledge of the particle polarizability is, in fact, insufficient for solving the problem at hand. The shape of the particles is also important and can not be disregarded.

Another way to look at this is the following. The polarizability  $\alpha$  defines the response of a particle to an external electric field which is almost uniform over the particle volume. However, in an infinite three-dimensional lattice, the electric field is not uniform over the particle volume, no matter how small the particle is. This is because the lattice Green's function  $W(\mathbf{R}, \mathbf{R}')$  given by (12) experiences an integrable divergence when  $\mathbf{R} = \mathbf{R}'$ . However, in the point-dipole model, we are attempting to evaluate this function exactly at  $\mathbf{R} = \mathbf{R}' = 0$ , which is not mathematically reasonable.

It appears that the only feasible approach to regularize the summation in (78) is to endow the particles with a finite volume, as was done, for example, in Ref. [14]. This would naturally lead to a modification of (78) in which the right-hand side is multiplied by a decaying function  $f(\mathbf{g})$ , ensuring convergence. Unfortunately, the exact form of  $f(\mathbf{g})$  strongly depends on the particle shape and size. If the regularization is carried out in a mathematically-consistent way, one would end up with a set of equations that are identical to the equations obtained here, for the model of a continuous two-component medium.

Evidently, within the point-dipole model, one wishes to avoid introducing the particle shape and size. Then the only conceivable approach to regularization is simply to truncate the series in (78), by leaving only the  $\mathbf{g} = 0$  term in the summation, which leads to the eigenproblem

$$\frac{1}{\alpha_{\text{LL}}} \mathbf{d} = \frac{4\pi}{3h^3} K(\mathbf{q}) \mathbf{d} . \quad (80)$$

Regularization of this type is, in fact, appropriate for small spherical particles. If one also uses the quasistatic polarizability of a sphere of radius  $a$ , namely,

$$\alpha_{\text{LL}} = a^3 \frac{\epsilon_a - \epsilon_b}{\epsilon_a + 2\epsilon_b} , \quad (81)$$

then (80) becomes equivalent to the Clausius-Mossotti relation and the EMT that follows from it is the standard Maxwell-Garnett approximation.

One may be tempted to forget about the limits of applicability of Eq. (80). In other words, once (80) is derived, it is technically possible to use it with *any* polarizability  $\alpha_{\text{LL}}$ . The latter can be obtained independently, i.e., by solving the Laplace equation for a single isolated particle of arbitrary shape. Unfortunately, this approach is mathematically inconsistent. Eq. (80) was derived from (78) by applying a regularization method which is only appropriate for small spheres. Applying (80) to particles of nonspherical shape is likely to result in errors.

In summary, the model of point dipoles is capable of reproducing the standard Maxwell-Garnett mixing rule for small spheres. Radiative corrections to this result can also be derived [15]. However, in three dimensions, the model breaks down and can not be used when a substantial deviation from the Maxwell-Garnett approximation is expected, i.e., for particles whose volume fraction is not small or whose shape is different from a sphere. In other words, the model does not provide a mathematically consistent way of computing the self-energy  $\Sigma$  which appears in equations (22) or (23) and is, therefore, usable only in the physical situations when  $\Sigma$  can be neglected. Nevertheless, we note that in systems of lower dimensionality (e.g., in nanoparticle chains), the point-dipole model is useful and can provide significant physical insights.

## 6. Continued-fraction expansion of the self-energy and the mean-field approximation

### 6.1. Abstract notations

In this section, we will find it convenient to rewrite Eqs. (19b) and (20) in Dirac notation. First, we note that, in order to recover all components of the tensor  $\Sigma$ , one must solve (19b) for three different right-hand sides:  $\mathbf{F}_0 = \hat{\mathbf{x}}$ ,  $\mathbf{F}_0 = \hat{\mathbf{y}}$  and  $\mathbf{F}_0 = \hat{\mathbf{z}}$ . To this end, we introduce a triplet of infinite-dimensional vectors  $|a_\beta\rangle$ , operators  $Q$ ,  $M$ ,  $W$ , and vectors  $|b_\beta\rangle$  ( $\beta = x, y, z$ ) according to

$$\langle \alpha \mathbf{g} | a_\beta \rangle = M(\mathbf{g}) \delta_{\alpha\beta} , \quad (82a)$$

$$\langle \alpha \mathbf{g} | Q | \alpha' \mathbf{g}' \rangle = \delta_{\mathbf{g}\mathbf{g}'} (1 - 3\hat{g}_\alpha \hat{g}_{\alpha'}) , \quad (82b)$$

$$\langle \alpha \mathbf{g} | M | \alpha' \mathbf{g}' \rangle = \delta_{\alpha\alpha'} M(\mathbf{g} - \mathbf{g}') , \quad (82c)$$

$$W = QM , \quad (82d)$$

$$|b_\beta\rangle = Q |a_\beta\rangle . \quad (82e)$$

Note that  $Q$  is diagonal in the index  $\mathbf{g}$ ,  $M$  is diagonal in the index  $\alpha$ , but the product of the two,  $W = QM$ , is not diagonal. We must also keep in mind that the index  $\mathbf{g}$  in

the above equations is not allowed to take the zero value. We further define the vectors  $|F_\beta\rangle$  as the solutions to

$$(1/\rho\chi - W)|F_\beta\rangle = |b_\beta\rangle. \quad (83)$$

The above equation is equivalent to the set of equations (19b). The tensor elements of  $\Sigma$  are defined by

$$\Sigma_{\alpha\beta} = \langle a_\alpha | F_\beta \rangle = \langle a_\alpha | (1/\rho\chi - W)^{-1} | b_\beta \rangle = \langle a_\alpha | (1/\rho\chi - QM)^{-1} Q | a_\beta \rangle. \quad (84)$$

It can be seen that  $\Sigma$  is computed as the resolvent of the operator  $W = QM$  and plays the role of the self-energy which accounts for interactions between the inclusions.

### 6.2. Mean-field approximation

The mean-field approximation is often misunderstood. In particular, it is unrelated to Maxwell-Garnett theory. Rather, it allows one to replace certain operators by appropriately chosen scalar multiples of the identity. The approximation reproduces the exact zeroth and first moments of the resolvent and serves as the first-order approximation in its continued-fraction expansion. Here the approximation is explained following Berry and Percival [30].

Let us seek the solution to Eq. (83) in the form  $|F_\beta\rangle = \lambda|b_\beta\rangle$ , where  $\lambda$  is a scalar to be determined. Upon substitution of this ansatz into (83), we obtain the equation

$$(1/\rho\chi - 1/\lambda)|b_\beta\rangle = W|b_\beta\rangle. \quad (85)$$

Because  $|b_\beta\rangle$  is, generally, not an eigenvector of  $W$ , there is no such value of  $\lambda$  for which Eq. (85) would hold. The best we can hope for is that a *projection* of this equation onto a given vector would hold for some  $\lambda$ . Since we are interested not in the whole vector  $|F_\beta\rangle$  but in its projection onto  $|a_\alpha\rangle$ , it seems reasonable to project Eq. (85) onto the latter. This yields

$$\lambda = \frac{\rho\chi}{1 - \rho\chi \langle a_\alpha | W | b_\beta \rangle / \langle a_\alpha | b_\beta \rangle}, \quad (86)$$

and the corresponding mean-field approximation for the self-energy is

$$\Sigma_{\alpha\beta} = \frac{\rho\chi \langle a_\alpha | b_\beta \rangle}{1 - \rho\chi \langle a_\alpha | W | b_\beta \rangle / \langle a_\alpha | b_\beta \rangle} = \frac{\rho\chi \langle a_\alpha | Q | a_\beta \rangle}{1 - \rho\chi \langle a_\alpha | Q M Q | a_\beta \rangle / \langle a_\alpha | Q | a_\beta \rangle}. \quad (87)$$

As was mentioned in Sec. 3.3, the matrix element

$$\langle a_\alpha | Q | a_\beta \rangle = \sum_{\mathbf{g} \neq 0} [M(-\mathbf{g})Q(\mathbf{g})M(\mathbf{g})]_{\alpha\beta} \quad (88)$$

is identically zero for inclusions with cubic symmetry (in three-dimensional composites) so that Eq. (87) yields zero and is not useful. In this case, a non-vanishing mean-field

approximation is obtained by “shifting” the solution according to  $|F_\beta\rangle = \rho\chi|b_\beta\rangle + |F'_\beta\rangle$ . The self-energy is then given by  $\Sigma_{\alpha\beta} = \langle a_\alpha|F'_\beta\rangle$  and  $|F'_\beta\rangle$  satisfies

$$(1/\rho\chi - W)|F'_\beta\rangle = \rho\chi W|b_\beta\rangle. \quad (89)$$

The mean-field approximation for the “shifted” equation (89) is

$$\Sigma_{\alpha\beta} = \frac{(\rho\chi)^2 \langle a_\alpha|QM|a_\beta\rangle}{1 - \rho\chi \langle a_\alpha|(QM)^2 Q|a_\beta\rangle / \langle a_\alpha|QM|a_\beta\rangle}. \quad (90)$$

### 6.3. Continued-fraction expansion of the self-energy

Continued-fraction expansions (CFEs) are very useful in physics [31, 32]. The mathematical underpinning of all CFEs is the theory of the correspondence between the formal Laurent series of meromorphic functions and certain continued fractions [33]. There exists a deep mathematical relation between CFEs and the problem of moments, that is, the problem of finding a distribution from knowledge of its moments.

CFEs can be derived in different ways. Haydock [31] has employed the Lanczos recursion to transform a certain Hamiltonian to tridiagonal form. A diagonal element of the inverse of a tridiagonal matrix can be written as a J-fraction (a continued fraction of Jacobi type). In Ref. [31], this procedure was applied to a Hermitian operator to compute a diagonal matrix element of the resolvent. In this paper, the operator  $W$  in (83) or (84) is not symmetric or Hermitian and we are interested in off-diagonal elements of the resolvent. Therefore, the numerical procedure used by Haydock is not directly applicable. Perhaps, it can be generalized to become applicable to the problem at hand; we have not explored this possibility. Instead, we will derive a CFE for the right-hand side of Eq. (84) from the following theorem which does not require any symmetry properties of the operators involved, yields a CFE for arbitrary off-diagonal elements, and, to the best of our knowledge, has not been reported in the literature. The resultant expansion will be an S-fraction (a continued fraction of Stieltjes type). Note that an S-fraction can always be transformed into a J-fraction by the so-called equivalence transformation.

**Theorem 1** *Let  $W$  be a linear operator acting on the Hilbert space  $\mathcal{H}$  and  $\mathcal{Z}$  be a complex number. Suppose that  $|\phi\rangle, |\psi\rangle \in \mathcal{H}$ . If (i)  $\langle\phi|\psi\rangle \neq 0$  and (ii)  $\mathcal{Z}$  is such that  $(\mathcal{Z} - W)^{-1}$  exists, then*

$$\langle\phi|(\mathcal{Z} - W)^{-1}|\psi\rangle = \frac{\mathcal{Z}^{-1}\langle\phi|\psi\rangle}{1 - \frac{\langle\phi|(\mathcal{Z} - WT)^{-1}W|\psi\rangle}{\langle\phi|\psi\rangle}}, \quad (91)$$

where

$$T = 1 - \frac{|\phi\rangle\langle\psi|}{\langle\psi|\phi\rangle}. \quad (92)$$

The proof is given in Appendix B. Note that (91) has a finite limit when  $\mathcal{Z} \rightarrow 0$ .

The factor  $\langle \phi | (\mathcal{Z} - WT)^{-1} W | \psi \rangle$  in the denominator of (91) can be written as  $\langle \phi | (\mathcal{Z} - W_1)^{-1} | \psi_1 \rangle$ , where  $W_1 = WT$  and  $|\psi_1\rangle = W|\psi\rangle$ . The formula (91) can now be applied to  $\langle \phi | (\mathcal{Z} - W_1)^{-1} | \psi_1 \rangle$ , and so on iteratively. After some manipulation, this yields the following expansion:

$$\langle \phi | (\mathcal{Z} - W)^{-1} | \psi \rangle = \frac{\mu_1}{\mathcal{Z} - \frac{\mu_2}{1 - \frac{\mu_3}{\mathcal{Z} - \dots}}} , \quad (93)$$

Note the interlacing factors of  $\mathcal{Z}$  and 1. The coefficients  $\mu_j$  ( $j = 1, 2, \dots$ ) are obtained from a three-point recursion. Namely, starting from  $|\psi_0\rangle = 0$ ,  $|\psi_1\rangle = |\psi\rangle$  and  $\mu_1 = \langle \phi | \psi \rangle$ , we compute for  $j = 1, 2, \dots$

$$|\psi_{j+1}\rangle = W \left( |\psi_j\rangle - \mu_j |\psi_{j-1}\rangle \right) , \quad \mu_{j+1} = \frac{\langle \phi | \psi_{j+1} \rangle}{\langle \phi | \psi_j \rangle} . \quad (94)$$

To obtain a CFE of the right-hand side of Eq. (84), we identify  $\mathcal{Z} = 1/\rho\chi$ ,  $W = QM$ ,  $|\phi\rangle = |a_\alpha\rangle$  and  $|\psi\rangle = |b_\beta\rangle = Q|a_\beta\rangle$ .

With the above substitutions taken into account, it transpires that the coefficients  $\mu_j$  are determined only by the geometry of the composite. Once a set of  $\mu_j$  have been found for a given geometry, the effective medium parameters can be easily computed for any material parameters of the composite constituents. This is a characteristic feature of a spectral theory and the CFE (93) is, in fact, a spectral representation of the self-energy  $\Sigma$ .

Finally, we note that, in the case of three-dimensional composites with cubic symmetry, the first condition of the Theorem does not hold (when the theorem is applied directly to (84)). In this case, one can build a CFE starting from the “shifted” equation (89).

## 7. Numerical simulations

### 7.1. General setup

Numerical simulations have been performed for a two-dimensional composite. The composite is periodic in the  $xy$  plane while the inclusions form infinitely-long fibers which are oriented parallel to the  $z$ -axis and can have different cross sections. The case when the electric field is parallel to the fibers is not considered here, since this polarization results in a simple arithmetic average of the type (31). However, when the electric field is polarized in the  $xy$  plane, the homogenization problem is nontrivial and can be numerically challenging. We will consider inclusions with circular and square cross sections, as is illustrated in Fig. 4. The functions  $M(\mathbf{g})$  for these shapes are given in Appendix A.

It is assumed that the host medium is vacuum and the inclusions are metallic and characterized by a frequency-dependent Drude permittivity of the form

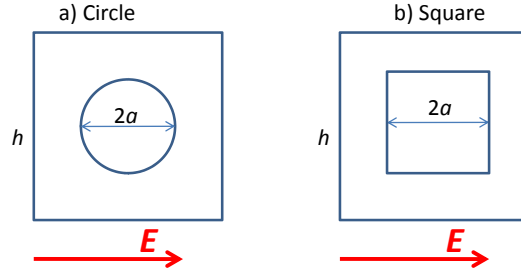


**Figure 4.** (color online) Two types of elementary cells used in numerical simulations.

$$\epsilon_a = 1 - \frac{3\omega_F}{\omega(\omega + i\gamma)}, \quad \epsilon_b = 1. \quad (95)$$

In Eq. (95),  $\omega_F = \omega_p/\sqrt{3}$  is the Frohlich frequency,  $\omega_p$  is the plasma frequency, and  $\gamma$  is the Drude relaxation constant. We will compute the effective permittivity of the composite  $\epsilon^{\text{eff}}$  as a function of frequency for  $0.1 \leq \omega/\omega_F \leq 2$  and for the fixed ratio  $\gamma/\omega_F = 0.1$ . It is assumed that, for all frequencies used in the simulations, the basic condition for the validity of a standard EMT,  $k_0 h, qh \ll 1$ , is satisfied.

Numerical simulations will be performed by truncating the infinite set of equations (19b) so that the vectors  $\mathbf{g}$  fill the box

$$-2\pi L/h \leq g_x, g_y \leq 2\pi L/h, \quad (96)$$

where  $L$  is an integer. The total number of  $\mathbf{g}$ -vectors which satisfy the above inequality is  $(2L+1)^2$  and the total number of algebraic equations to be solved is  $N = 2[(2L+1)^2 - 1]$ , where we have accounted for the fact that the vector  $\mathbf{g} = 0$  is excluded in the set of equations (19b). It can be seen that  $N \rightarrow 8L^2$  when  $L \rightarrow \infty$ . In the simulations, we will use integer powers of 2 for  $L$ , up to  $L = 2^8 = 256$ . The latter case corresponds to  $N = 526,366$  equations.

The truncated set of equations (19b) can be solved by any direct numerical method. The computational complexity of direct methods is  $O(N^3)$  and the solution must be obtained anew for every frequency used (we sample the frequency at 200 equidistant points in the interval  $0.1 \leq \omega/\omega_F \leq 2$ ). This is time-consuming but possible for  $L \leq 64$ . For larger values of  $L$ , direct methods become impractical. We will use, therefore, the CFE of Sec. 6.3. The computational complexity of this expansion is  $O(j_{\text{max}} N^2)$ , where  $j_{\text{max}}$  is the order of truncation of the continued fraction. More specifically, the continued fraction is truncated by assuming that  $\mu_j = 0$  for  $j > j_{\text{max}}$ , so that only the first  $j_{\text{max}}$  coefficients are used in Eq. (93). For the problem at hand,  $j_{\text{max}} \approx 50$  will prove sufficient. Other iterative methods, such as the conjugate gradient method, also have computational complexity  $O(j_{\text{max}} N^2)$ ,  $j_{\text{max}}$  being the number of iterations. However, the computationally-intensive part of the conjugate-gradient solver (when applied to

Eq. (19b)) must be repeated for every value of  $\omega$ , while the coefficients  $\mu_j$  in (93) need to be computed only once for a given geometry.

The inclusions shown in Fig. 4 have cubic symmetry. As was discussed in Sec. 3.2, the self-energy  $\Sigma$  is reduced in this case to a scalar. As a result, the effective medium is isotropic in the  $xy$  plane. Of course, anisotropy can still be revealed if the polarization vector has a component along the  $z$ -axis. In the simulations reported below, we have computed  $\Sigma$  by solving Eqs. (19b) and using the definition (20). The effective permittivity for transversely-polarized waves was then computed by using Eq. (23).

## 7.2. Convergence and stability

The convergence of the CFE (93) with the truncation order of the continued fraction,  $j_{\max}$ , is illustrated in Fig. 5. Here the real and imaginary parts of the effective permittivity are plotted as functions of frequency. It can be seen that the convergence is very fast for circular inclusions and somewhat slower for square inclusions. In all cases,  $j_{\max} = 50$  is sufficient for convergence.

The three-point recurrence relation (94) is numerically unstable for large values of  $j$ . This is illustrated in Fig. 6. Shown in this figure are the coefficients  $\mu_j$  obtained on two different computers for the geometry described in the figure caption. The same code and input data were used in both cases. The coefficients from the two sets coincide for  $j \lesssim 50$  with high precision. However, differences start to appear at  $j \sim 50$  and, at  $j \sim 100$ , the coefficients are unreliable. The instability occurs when an iteration step in (94) asks for a relatively small difference of two large numbers and the numerical precision of the floating-point arithmetic is exceeded.

The instability illustrated in Fig. 6 appears to be troublesome but is, in fact, of little concern. This is illustrated in Fig. 7, which displays the effective permittivity computed by the CFE (93) for various truncation orders  $j_{\max}$ , and the same quantity computed by solving Eqs. (19b) directly. One of the sets of  $\mu_j$ 's displayed in Fig. 6 has been used for computing the data points for panels (a,b) of Fig. 7. Despite the instability, the curves with  $j_{\max} = 50$  and  $j_{\max} = 100$  are indistinguishable and very close to the data points obtain by direct inversion of (19b). Thus, the unreliable coefficients  $\mu_j$  do not influence the final result. This is one of the nice properties of all CFEs: a numerical instability does not result in numerical imprecision. It is true that increasing the truncation order beyond  $j_{\max} = 50$  is not useful, but it is not harmful either. This point and some related issues are discussed in more detail in Sec. 8 below.

Having established the convergence properties of the CFE, we next consider convergence with the size of the box,  $L$  (up to now, all plots have been computed for  $L = 64$ ). In Figs. 8,  $\epsilon^{\text{eff}}$  is plotted as functions of frequency for various values of the density,  $\rho$ , and the box size,  $L$ . Also shown in these figures are the results obtained from the generalized Maxwell-Garnett formula

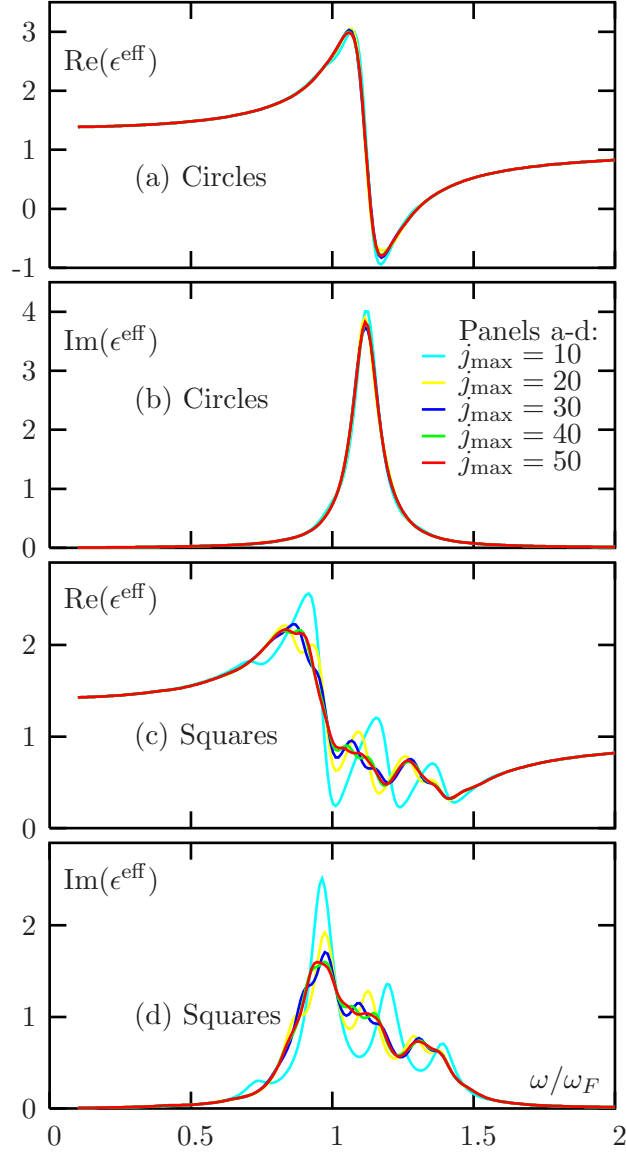


**Figure 5.** (color online) Convergence of the CFE (93) with the truncation order  $j_{\max}$  for circular (a,b) and quadratic (c,d) inclusions with the same volume density  $\rho = 0.16$ . The set of equations (19b) has been truncated using  $L = 64$ . In panels (a,b), the curves with  $j_{\max} = 30, 40, 50$  are indistinguishable.

$$\epsilon_{\nu} = \epsilon_b \frac{1 + \frac{2\rho}{3} \frac{\epsilon_a - \epsilon_b}{\epsilon_b + \nu(\epsilon_a - \epsilon_b)}}{1 - \frac{\rho}{3} \frac{(\epsilon_a - \epsilon_b)}{\epsilon_b + \nu(\epsilon_a - \epsilon_b)}}, \quad (97)$$

which applies to ellipsoids,  $\nu$  being the appropriate depolarization factor. In the case of three-dimensional spheres,  $\nu = 1/3$  and Eq. (97) coincides with Eq. (23) in which the self-energy  $\Sigma$  is set to zero. In the case of infinite circular cylinders, the depolarization factor which corresponds to the orthogonal electric polarization is  $\nu = 1/2$ .



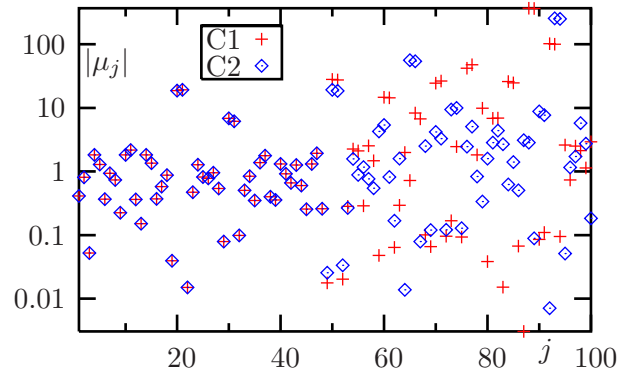


**Figure 6.** (color online) Absolute values of the coefficients  $\mu_j$  computed for circular inclusions with  $\rho = 0.16$  and  $L = 64$  on two different computers (C1 and C2). The same FORTRAN code and input data have been used in both cases.

Several conclusions can be drawn from Fig. 8. First, convergence is obtained for boxes of reasonable size. In all cases shown,  $L = 256$  yields very accurate results, and in some cases  $L = 64$  is sufficient. However, it is important to note that we have verified the convergence by doubling the size of the box. Determination of convergence by using linearly sampled values of  $L$ , (say,  $L = 10, 11, 12 \dots$ ) can be very misleading. This is a typical situation when boundary-value problems are solved numerically. Convergence must be established by at least doubling the size of the mesh used.

Second, it can be seen that convergence is faster for  $\rho = 0.32$  than for  $\rho = 0.16$ . Although the electromagnetic interaction is stronger in the second case, the faster convergence is to be expected. Indeed, the size of the box should be selected so that the sum rules (A.2) are satisfied with some reasonable precision, and that is achieved at smaller values of  $L$  for larger values of  $\rho$ . Even faster convergence is obtained for  $\rho = 0.64$  (data not shown). However, at the percolation threshold ( $\rho = \pi/4 \approx 0.79$  for circular inclusions), the convergence is relatively slow.

Third, the generalized Maxwell-Garnett formula (97) with  $\nu = 1/2$  yields a reasonable result for circular inclusions with  $\rho = 0.16$ . Even better agreement has been obtained for  $\rho = 0.08$  and  $\rho = 0.04$  (data not shown). However, as the size of circular inclusions increases, the Maxwell-Garnett approximation becomes less accurate. For square inclusion, the approximation is inaccurate even for very small values of  $\rho$ . In all cases, the electromagnetic interaction tends to shift the absorption peaks from the Maxwell-Garnett's prediction towards the lower frequencies. At  $\rho = 0.32$ , the effect is already quite pronounced.

### 7.3. Comparison of inclusions of various size

We finally compare the effective permittivity for circular and square inclusions of different sizes. The results are displayed in Fig. 9. In the case of circular inclusions, there exists a pronounced spectral peak which shifts towards lower frequencies when

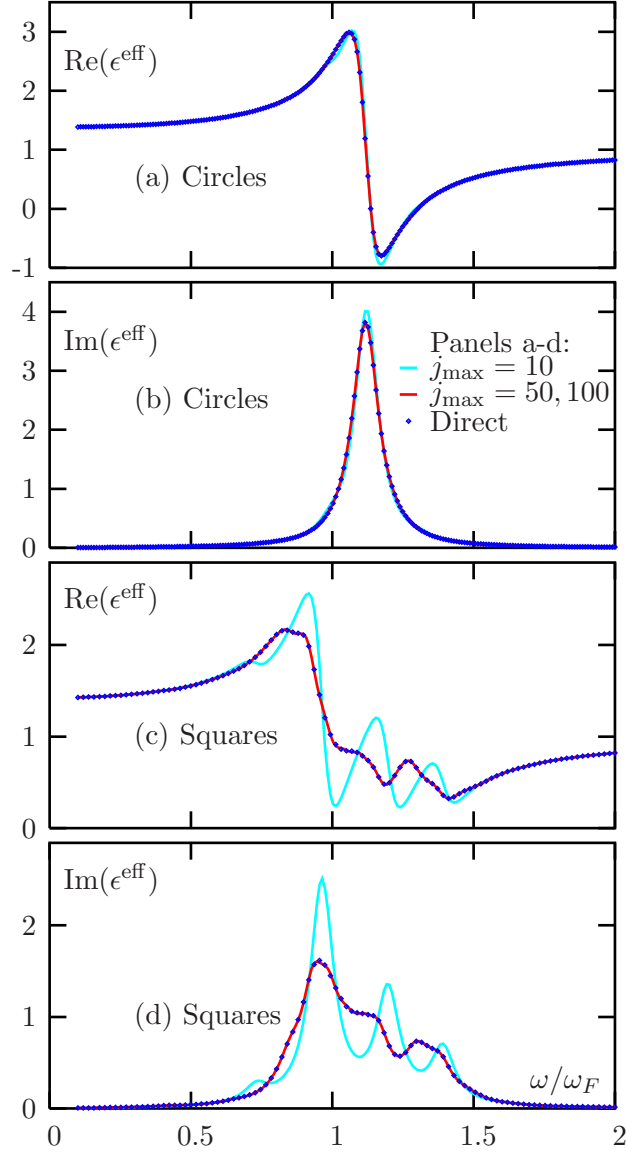


**Figure 7.** (color online) Effective permittivity of circular (a,b) and square (b,c) inclusions computed using the CFE (93) with the truncation orders  $j_{\text{max}} = 10, 50, 100$ , and by direct inversion of Eqs. (19b). In all cases,  $\rho = 0.16$  and  $L = 64$ . The data points for  $j_{\text{max}} = 50$  and  $j_{\text{max}} = 100$  are visually indistinguishable and, therefore, represented with the same curve.

$\rho$  is increased. However, once the inclusions touch (this happens at  $\rho = \pi/4 \approx 0.79$ , the single resonance is destroyed and a broad absorption band develops. The lower-frequency behavior of  $\epsilon^{\text{eff}}$  is in this case metallic, since the percolating sample is characterized by a nonzero static conductivity. This result can not be obtained within the Maxwell-Garnet approximation, or the Bruggemann approximation, even at a qualitative level.

The square inclusions do not touch for  $\rho < 1$ . Correspondingly, the low-frequency behavior of  $\epsilon^{\text{eff}}$  is not metallic even for large filling fractions, e.g., for  $\rho = 0.85$ .

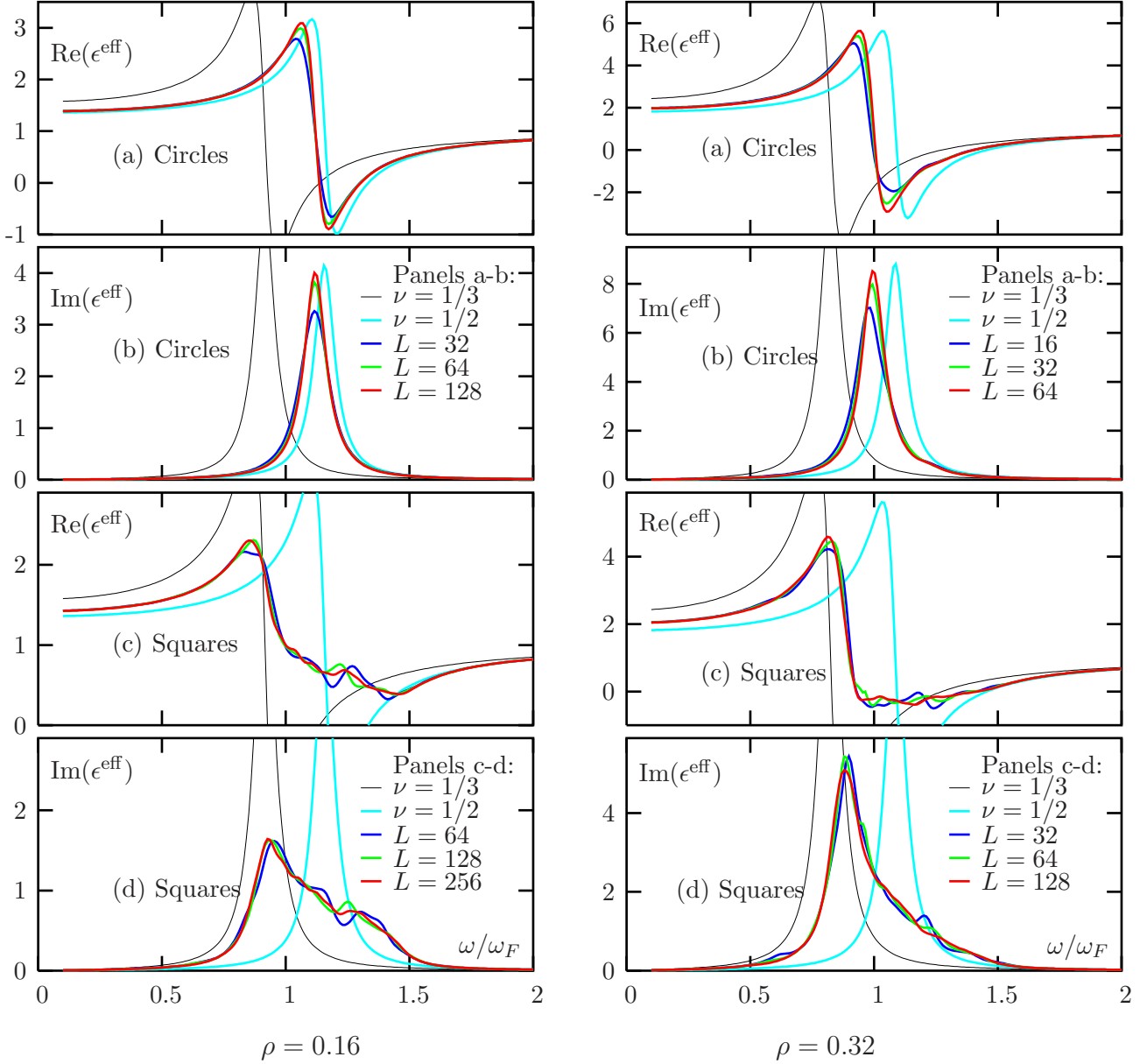


**Figure 8.** (color online) Left column: Convergence of the effective permittivity  $\epsilon^{\text{eff}}$  with the size of the box,  $L$ , for circular (a,b) and square (c,d) inclusions with  $\rho = 0.16$ . The curves labeled as  $\nu = 1/2$  and  $\nu = 1/3$  have been obtained from the generalized Maxwell-Garnett mixing formula (97) for the values of  $\nu$  indicated. Right column: same as in the left column but for  $\rho = 0.32$ .

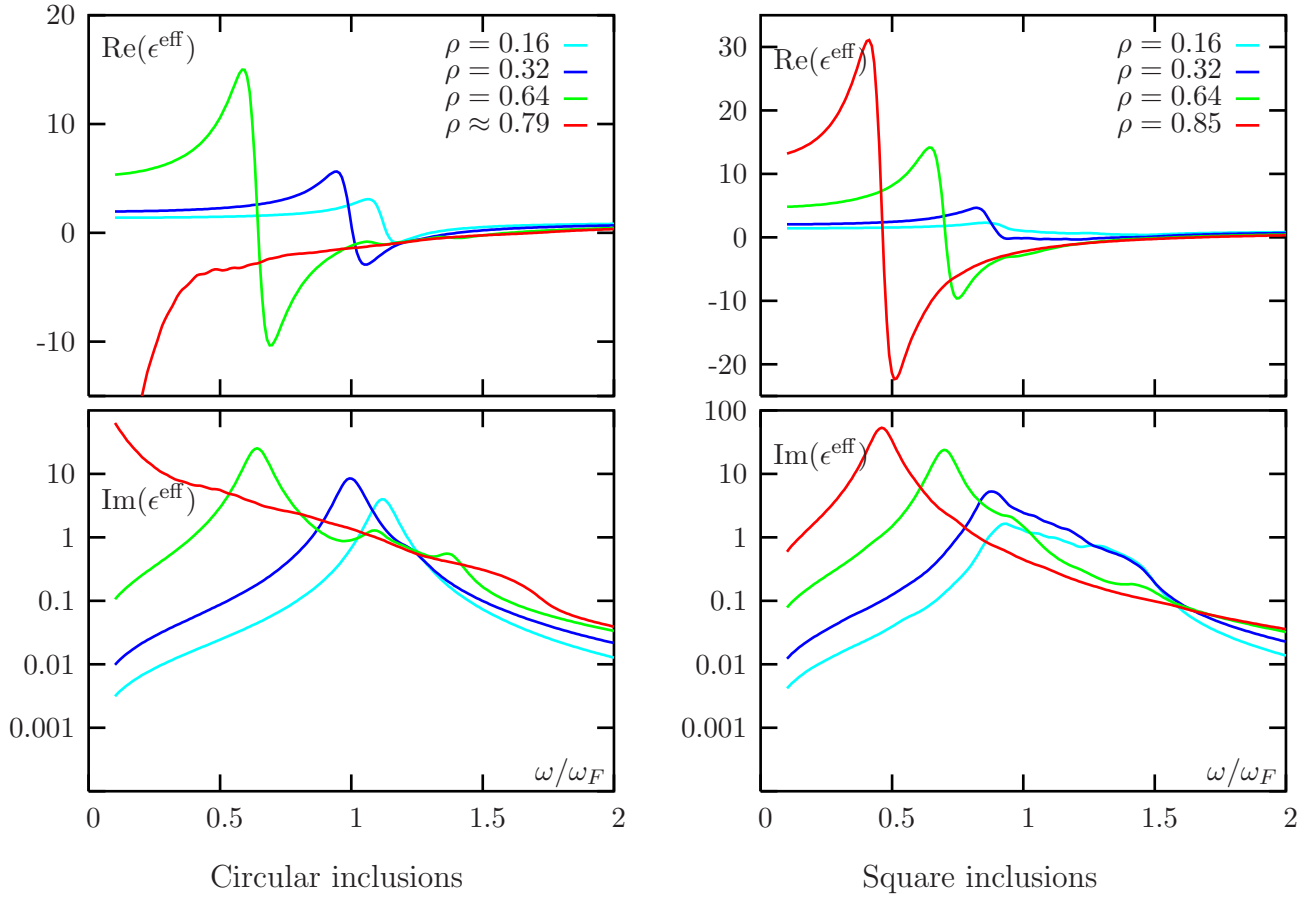


**Figure 9.** (color online) Effective permittivity for circular inclusions (left column) and square inclusions (right column) with different volume densities. For spherical inclusions, the case  $\rho \approx 0.79$  case to the percolation threshold (touching circles).

Interestingly, at relatively small values of  $\rho$ , the absorption spectrum forms a band with one main resonance and many minor resonances which are shifted towards the shorter waves. However, as  $\rho$  increases, the minor resonances become less pronounced. At  $\rho = 0.85$ , the spectrum is dominated by a single Lorentzian-type resonance. In the case of circular inclusions, the picture is somewhat different. A single Lorentzian resonance exists at small values of  $\rho$  and additional minor resonances develop as  $\rho$  increases. These additional resonances are clearly visible in the  $\rho = 0.64$  curve shown in the left column of Fig. 9.

## 8. Discussion

A few points that deserve additional discussion are addressed in this section, in no particular order.

### 8.1. Consideration of chirality

Although the general formalism of this paper allows one to take chiral media into consideration, all derivations which were brought to a logical conclusion have been carried out for the non-chiral case. This has provided a mathematical simplification, yet left untouched a wealth of interesting physical phenomena which are associated with chirality. This shortcoming will be addressed by us in the future.

### 8.2. 3D vs 2D simulations

So far, we have performed simulations only for 2D media. One can argue that in the 3D case the size of the algebraic problem would become so large as to render the method unusable. Of course, three-dimensional electromagnetic problems are always challenging. However, there is reason for optimism. Namely, the formula for the effective permittivity (23) uses the three-dimensional Maxwell-Garnett approximation as the point of departure. In other words, a nonzero value of  $\Sigma$  provides a correction to the three-dimensional Maxwell-Garnett formula. This happens to be true even for two-dimensional media. However, the three-dimensional Maxwell-Garnett formula is inaccurate in the 2D case even for very thin cylinders, as is clearly illustrated in Fig. 8. In the numerical simulations of Sec. 7 (for circular inclusions), a lot of effort was spent to compute accurately the self-energy  $\Sigma$  whose effect was, essentially, to transform the Maxwell-Garnett from a 3D to a 2D form.

In the case of small three-dimensional inclusions, one can expect a much faster convergence with  $L$ . For example, if the inclusions are small spheres, an accurate result is obtained by starting with  $\Sigma = 0$ . As the spheres increase in size, the Maxwell-Garnett approximation becomes less accurate and a nonzero value of  $\Sigma$  must be used. However, as we have seen in the numerical simulations, the required values of  $L$  are, in fact, smaller for larger sizes of the inclusions.

Mathematically, the above considerations are related to an interesting fact which was mentioned in Sec. 6. Namely, the matrix element  $\langle a_\alpha | Q | a_\beta \rangle$  is identically zero for three-dimensional cells with cubic symmetry. Consequently, the mean-field approximation and the continued-fraction expansion must be derived for the “shifted” equation (89). As a result, the mean-field formula (90) contains an overall factor of  $(\rho\chi)^2$  while in the 2D simulations of Sec. 7, this factor was equal to  $\rho\chi$ .

### 8.3. The case of small losses

The numerical simulations of Sec. 7 have been performed for a relatively large loss parameter,  $\gamma/\omega_F = 0.1$ . If this number is substantially reduced, the convergence with the truncation order of the continued fraction,  $j_{\max}$ , is expected to become slower. A general rule of thumb is that the truncation order should not be less than the number of clearly discernible peaks in the function  $\text{Im}\epsilon^{\text{eff}}(\omega)$  (the absorption spectrum). This is because the continued-fraction expansion truncated at the order  $j_{\max}$  captures correctly

the first  $j_{\max}$  moments of the above function. At sufficiently large values of  $j$ , the three-point recursion (94) becomes numerically unstable, as is illustrated in Fig. 6. If the required value of  $j_{\max}$  is larger than the value of  $j$  at which the onset of numerical instability occurs, then the continued fraction expansion will not yield an accurate result.

The situation outlined above is common for all iterative methods. For example, the convergence of the conjugate-gradient method becomes extremely slow for small ratios of  $\gamma/\omega_F$ ; at some point, the recurrence relations used in the conjugate-gradient iterations also become numerically unstable. One can hope to improve stability by deriving a CFE which utilizes the Lanczos recursion of Ref. [31] instead of (94), although a comparative study of stability of these two recursions have not been performed. Whether this is a feasible approach, remains to be investigated.

## 9. Summary

We can draw the following conclusions:

- (i) We have provided an efficient approach to computing the effective permittivity of periodic composites. The convergence and numerical stability of the method have been thoroughly investigated. One conclusion that can be reached is that convergence must be verified by at least doubling the size of the box in which the reciprocal lattice vectors are stored.
- (ii) A medium constructed from nonmagnetic components is also nonmagnetic in the limit in which it can be considered as electromagnetically homogeneous. This result is in line with the original arguments of Bohren [6], simulations of Menzel *et al.* [9] and the more formal mathematical theory of Wellander and Kristensson [34], but contradicts the results of extended EMTs.
- (iii) The model of point-like polarizable particles is ill-suited for homogenization of three-dimensional periodic composites due to inherent divergences. The point-dipole approximation can be still a useful theoretical tool for studying systems in lower dimensions.

It is appropriate to conclude this paper by quoting from the 1986 paper by C.F. Bohren [6], whose arguments against the use of extended EMTs have been neither refuted nor heeded: “The conclusion is inescapable, although perhaps unpalatable, that if problems of absorption and scattering by nonhomogeneous particles must be solved, and if heterogeneities are not electric dipoles, then we must abandon the fruitless search for extended effective-medium theories and tackle such problems by other methods.”

## Acknowledgments

The authors are grateful to Profs. Shari Moskow and Igor Tsukerman for valuable discussions. This work was supported by the NSF under Grant No. DMR0425780 and by the USAFOSR under Grant No. FA9550-07-1-0096.

## References

- [1] C. R. Simovski, *Opt. Spectrosc.* **107**, 766 (2009).
- [2] C. F. Bohren, *J. Nanophotonics* **3**, 039501 (2009).
- [3] G. A. Niklasson, C. G. Granqvist, and O. Hunderi, *Appl. Opt.* **20**, 26 (1981).
- [4] W. T. Doyle, *Phys. Rev. B* **39**, 9852 (1989).
- [5] D. Felbacq and G. Bouchitte, *New J. Phys.* **7**, 159 (2005).
- [6] C. F. Bohren, *J. Atmospheric Sci.* **43**, 468 (1986).
- [7] R. Rupp, *Opt. Comm.* **182**, 273 (2000).
- [8] R. G. Barrera and A. Garcia-Valenzuela, *J. Opt. Soc. Am. A* **20**, 296 (2003).
- [9] C. Menzel, T. Paul, C. Rockstuhl, T. Pertsch, S. Tretyakov, and F. Lederer, *Phys. Rev. B* **81**, 035320 (2010).
- [10] J. D. Baena, L. Jelinek, R. Marques, and M. Silveirinha, *Phys. Rev. A* **78**, 013842 (2008).
- [11] M. G. Silveirinha, *New J. Phys.* **11**, 113016 (2009).
- [12] C. Menzel, C. Rockstuhl, T. Paul, F. Lederer, and T. Pertsch, *Phys. Rev. B* **77**, 195328 (2008).
- [13] J. B. Pendry, *Phys. Rev. Lett.* **85**, 3966 (2000).
- [14] J. E. Sipe and J. Van Kranendonk, *Phys. Rev. A* **9**, 1806 (1974).
- [15] B. T. Draine and J. Goodman, *Astrophys. J.* **405**, 685 (1993).
- [16] P. A. Belov and C. R. Simovski, *Phys. Rev. E* **72**, 026615 (2005).
- [17] D. J. Bergman, *Phys. Rep.* **43**, 377 (1978).
- [18] D. J. Bergman, *J. Phys.: Condens. Matter* **12**, 4947 (1979).
- [19] D. J. Bergman, *Phys. Rev. B* **19**, 2359 (1979).
- [20] A. A. Krokhin, P. Halevi, and J. Arriaga, *Phys. Rev. B* **65**, 115208 (2002).
- [21] A. A. Krokhin and E. Reyes, *Phys. Rev. Lett.* **93**, 023904 (2004).
- [22] F. J. G. Abajo, *Rev. Mod. Phys.* **79**, 1267 (2007).
- [23] V. A. Markel and J. C. Schotland, *J. Opt.* **12**, 015104 (2010).
- [24] A. A. Maradudin and D. L. Mills, *Phys. Rev. B* **11**, 1392 (1975).
- [25] G. D. Mahan and G. Obermair, *Phys. Rev.* **183**, 834 (1969).
- [26] W. Lamb, D. M. Wood, and N. W. Ashcroft, *Phys. Rev. B* **21**, 2248 (1980).
- [27] B. T. Draine, *Astrophys. J.* **333**, 848 (1988).
- [28] V. A. Markel, *J. Mod. Opt.* **39**, 853 (1992).
- [29] V. A. Markel, *J. Opt. Soc. Am. B* **12**, 1783 (1995).
- [30] M. V. Berry and I. C. Percival, *Optica Acta* **33**, 577 (1986).
- [31] R. Haydock, *The Recursive Solution of the Schrodinger Equation*, in *Solid State Physics*, Vol. 35 (Academic Press, 1980).
- [32] V. A. Markel, V. N. Pustovit, S. V. Karpov, A. V. Obuschenko, V. S. Gerasimov, and I. L. Isaev, *Phys. Rev. B* **70**, 054202 (2004).
- [33] W. B. Jones and W. J. Thron, *Continued Fractions. Analytic Theory and Applications*, (Addison-Wesley, 1980).
- [34] N. Wellander and G. Kristensson, *SIAM J. Appl. Math.* **64**, 170 (2003).

Appendix A. Mathematical properties of  $M(\mathbf{g})$  and some special cases

From the definition (18), it follows that

$$M(0) = 1 \ , \quad M(-\mathbf{g}) = M^*(\mathbf{g}) \ . \quad (\text{A.1})$$

For the case of inclusions whose center of symmetry coincides with the center of the unit cell, we have  $M(-\mathbf{g}) = M(\mathbf{g})$  and, therefore,  $M(\mathbf{g})$  is real. If the center of symmetry is displaced by a vector  $\boldsymbol{\xi}$ , the function  $\mathbf{M}(\mathbf{g})$  is transformed according to

$$\mathbf{M}(\mathbf{g}) \rightarrow \exp(-i\boldsymbol{\xi} \cdot \mathbf{g})\mathbf{M}(\mathbf{g}).$$

By applying the Poisson summation formula, we can derive the following sum rules:

$$\sum_{\mathbf{g}} M(\mathbf{g}) = \begin{cases} 1/\rho, & 0 \in \Omega, \\ 0, & 0 \notin \Omega, \end{cases} \quad (\text{A.2a})$$

$$\sum_{\mathbf{g}} M(-\mathbf{g})M(\mathbf{g}) = \frac{1}{\rho}, \quad (\text{A.2b})$$

$$\sum_{\mathbf{g}'} M(\mathbf{g} - \mathbf{g}')M(\mathbf{g}') = \frac{1}{\rho}M(\mathbf{g}). \quad (\text{A.2c})$$

These equations hold for inclusions of arbitrary shape.

Now define a complimentary function  $N(\mathbf{g})$  by

$$N(\mathbf{g}) = \frac{1}{h^3 - V} \int_{C \setminus \Omega} \exp(-i\mathbf{g} \cdot \mathbf{R}) d^3R. \quad (\text{A.3})$$

Here  $C$  denotes the unit cell and  $C \setminus \Omega$  is the region complimentary to the inclusion. It can be seen that  $N(\mathbf{g})$  has all the properties of  $M(\mathbf{g})$  with the substitution  $\rho \rightarrow 1 - \rho$ . Additionally, the functions  $M(\mathbf{g})$  and  $N(\mathbf{g})$  are related by

$$\rho M(\mathbf{g}) + (1 - \rho)N(\mathbf{g}) = \delta_{\mathbf{g}0}. \quad (\text{A.4})$$

From this, we obtain the low and high-density limits:

$$\lim_{\rho \rightarrow 0} N(\mathbf{g}) = \lim_{\rho \rightarrow 1} M(\mathbf{g}) = \delta_{\mathbf{g}0}. \quad (\text{A.5})$$

Of course, the high-density limit is unreachable for most regular shapes (with the exception of cubes). For example, in the case of spheres, the maximum allowed value of  $\rho$  is  $\pi/6$ .

Some special cases of  $M(\mathbf{g})$  are given below. For an inclusion in the shape of either a 3D sphere or a 2D circle of radius  $a \leq h/2$ ,

$$M_{3D}(\mathbf{g}) = \frac{3[\sin(ga) - ga \cos(ga)]}{(ga)^3}, \quad M_{2D}(\mathbf{g}) = \frac{2J_1(ga)}{ga}, \quad (\text{A.6})$$

where  $J_1(x)$  is the cylindrical Bessel function of the first kind. For a parallelepiped or rectangle centered at the origin with all faces parallel to the crystallographic planes and sides of length  $2a_x$ ,  $2a_y$  and  $2a_z$ ,

$$M_{3D}(\mathbf{g}) = \frac{\sin(g_x a_x)}{g_x a_x} \frac{\sin(g_y a_y)}{g_y a_y} \frac{\sin(g_z a_z)}{g_z a_z}, \quad M_{2D}(\mathbf{g}) = \frac{\sin(g_x a_x)}{g_x a_x} \frac{\sin(g_y a_y)}{g_y a_y}. \quad (\text{A.7})$$



## Appendix B. Proof of Theorem 1

### B.1. An equivalence transformation

To derive the equality (91), we first introduce some notation. Let

$$\varepsilon \equiv \langle \phi | \psi \rangle , \quad (\text{B.1a})$$

$$P \equiv |\psi\rangle\langle\phi| , \quad (\text{B.1b})$$

$$R(\mathcal{Z}; A) \equiv (\mathcal{Z} - A)^{-1} , \quad (\text{B.1c})$$

$$B \equiv R(\mathcal{Z}; W)W , \quad (\text{B.1d})$$

$$\sigma \equiv \langle \phi | R(\mathcal{Z}; W) | \psi \rangle . \quad (\text{B.1e})$$

Here  $R(\mathcal{Z}; A)$  is the resolvent of the linear operator  $A$  and  $\mathcal{Z}$  is a complex number. In the new notation, the operator  $T$  defined in (92) takes the form

$$T = 1 - \frac{1}{\varepsilon} P \quad (\text{B.2})$$

and Eq. (91) is rewritten as

$$\sigma = \frac{1}{\mathcal{Z}} \frac{\varepsilon}{1 - \varepsilon^{-1} \langle \phi | R(\mathcal{Z}; WT) W | \psi \rangle} . \quad (\text{B.3})$$

Note that, by the first hypothesis of the Theorem,  $\varepsilon \neq 0$ .

We now write the following chain of equalities in which the second hypothesis of the Theorem, namely, that  $R(\mathcal{Z}; W)$  exists, has been used:

$$\begin{aligned} R(\mathcal{Z}; WT) &= (\mathcal{Z} - WT)^{-1} = \left( \mathcal{Z} - W + \frac{1}{\varepsilon} WP \right)^{-1} = \left( R^{-1}(\mathcal{Z}; W) + \frac{1}{\varepsilon} WP \right)^{-1} \\ &= \left[ R^{-1}(\mathcal{Z}; W) \left( 1 + \frac{1}{\varepsilon} R(\mathcal{Z}; W) WP \right) \right]^{-1} = \varepsilon [\varepsilon + R(\mathcal{Z}; W) WP]^{-1} R(\mathcal{Z}; W) . \end{aligned} \quad (\text{B.4})$$

Using the last equality in (B.4) and the notation (B.1d), we rewrite (B.3) identically as

$$\sigma = \frac{1}{\mathcal{Z}} \frac{\varepsilon}{1 - \langle \phi | (\varepsilon + BP)^{-1} B | \psi \rangle} . \quad (\text{B.5})$$

### B.2. A useful identity

Below, we will frequently use the following identity:

$$\langle \phi | B | \psi \rangle = \mathcal{Z} \sigma - \varepsilon . \quad (\text{B.6})$$

The above equation is easily derived by noting that

$$\begin{aligned}\langle \phi | B | \psi \rangle &= \langle \phi | (\mathcal{Z} - W)^{-1} W | \psi \rangle \\ &= \langle \phi | (\mathcal{Z} - W)^{-1} (W - \mathcal{Z}) | \psi \rangle + \mathcal{Z} \langle \phi | (\mathcal{Z} - W)^{-1} | \psi \rangle = -\varepsilon + \mathcal{Z}\sigma .\end{aligned}\quad (\text{B.7a})$$

### B.3. The main derivation

To proceed, we need to express the operator  $(\varepsilon + BP)^{-1}$ , which appears in the right-hand side of (B.5), in a more tractable form. To this end, consider the equation

$$(\varepsilon + BP)|x\rangle = |\xi\rangle , \quad (\text{B.8})$$

where  $|x\rangle$  is viewed as the unknown and  $|\xi\rangle \neq 0$ . Using the definition of  $P$  (B.1b), we transform (B.8) to

$$\varepsilon|x\rangle + B|\psi\rangle\langle\phi|x\rangle = |\xi\rangle , \quad (\text{B.9})$$

project the result onto  $|\phi\rangle$ , and find that

$$\langle\phi|x\rangle = \frac{\langle\phi|\xi\rangle}{\varepsilon + \langle\phi|B|\psi\rangle} . \quad (\text{B.10})$$

We now use the previously-derived identity (B.6) in the right-hand side of (B.10) to obtain

$$\langle\phi|x\rangle = \frac{\langle\phi|\xi\rangle}{\mathcal{Z}\sigma} . \quad (\text{B.11})$$

Upon substitution of (B.11) into (B.9), we find the solution to (B.8) or (B.9), namely,

$$|x\rangle = \frac{1}{\varepsilon} \left( 1 - \frac{B|\psi\rangle\langle\phi|}{\mathcal{Z}\sigma} \right) |\xi\rangle . \quad (\text{B.12})$$

Since the vector  $|\xi\rangle$  in (B.8) is arbitrary, we conclude that

$$(\varepsilon + BP)^{-1} = \frac{1}{\varepsilon} \left( 1 - \frac{B|\psi\rangle\langle\phi|}{\mathcal{Z}\sigma} \right) . \quad (\text{B.13})$$

This equality can be verified directly by substitution.

### B.4. Putting everything together

We can now put everything together and obtain (B.5). From (B.13), we have

$$\langle\phi|(\varepsilon + BP)^{-1} = \frac{1}{\varepsilon} \left( 1 - \frac{\langle\phi|B|\psi\rangle}{\mathcal{Z}\sigma} \right) \langle\phi| = \frac{\langle\phi|}{\mathcal{Z}\sigma} , \quad (\text{B.14})$$

where we have, again, used (B.6). Now, we can write

$$\langle\phi|(\varepsilon + BP)^{-1}B|\psi\rangle = \frac{\langle\phi|B|\psi\rangle}{\mathcal{Z}\sigma} = 1 - \frac{\varepsilon}{\mathcal{Z}\sigma} . \quad (\text{B.15})$$

Upon substitution of this result into the right-hand side of (B.5), we find that the latter is, indeed, an identity, and so are (B.3) and (91).